JCI The Journal of Clinical Investigation

BET bromodomain inhibition attenuates cardiac phenotype in myocyte-specific Lamin A/C-deficient mice

Gaelle Auguste, … , Priyatansh Gurha, Ali J. Marian

J Clin Invest. 2020. https://doi.org/10.1172/JCI135922.

Research In-Press Preview Cardiology

Mutation in the *LMNA* gene, encoding Lamin A/C, cause a diverse group of diseases called laminopathies. Cardiac involvement is the major cause of death and manifests as dilated cardiomyopathy (DCM), heart failure, arrhythmias, and sudden death. There is no specific therapy for LMNA-associated cardiomyopathy. We report that deletion of *Lmna* in cardiac myocytes in mice leads to severe cardiac dysfunction, conduction defect, ventricular arrhythmias, fibrosis, apoptosis, and premature death within 4 weeks. The phenotype is similar to LMNA-associated cardiomyopathy in humans. RNA sequencing, performed prior to the onset of cardiac dysfunction, led to identification of 2,338 differentially expressed genes (DEGs) in *Lmna*-deleted cardiac myocytes. DEGs predicted activation of bromodomain-containing protein 4 (BRD4), a regulator of chromatin-associated proteins and transcription factors, which was confirmed by complementary approaches, including chromatin immunoprecipitation-sequencing. Daily injection of JQ1, a specific BET bromodomain inhibitor partially reversed the DEGs, including those encoding secretome, improved cardiac function, abrogated cardiac arrhythmias, fibrosis, and apoptosis, and prolonged the median survival time by 2-fold in the myocyte-specific *Lmna*-deleted mice. The findings highlight the important role of LMNA in cardiac myocyte and identify BET bromodomain inhibition as a potential therapeutic target in LMNA-associated cardiomyopathy, for which there is no specific effective therapy.

BET Bromodomain Inhibition Attenuates Cardiac Phenotype in Myocyte-Specific Lamin A/C-Deficient Mice

Gaelle Auguste [1], Leila Rouhi[1], Scot J Matkovich [2], Cristian Coarfa [3], Matthew J. Robertson [3], Grazyna Czernuszewicz [1], Priyatansh Gurha [1], Ali J. Marian[1 *]

[1] Center for Cardiovascular Genetics, Institute of Molecular Medicine and Department of Medicine, University of Texas Health Sciences Center at Houston, Texas 77030

[2] Washington University, Saint Louis, MO

[3] Baylor College of Medicine, Houston, TX 77030

None of the authors declares a conflict of interest.

*** Address for Correspondence:**
AJ Marian, M.D.
Center for Cardiovascular Genetics
6770 Bertner Street
Suite C900A
Houston, TX 77030
713 500 2350
Ali.J.Marian@uth.tmc.edu

Abstract

Mutation in the *LMNA* gene, encoding Lamin A/C, cause a diverse group of diseases called laminopathies. Cardiac involvement is the major cause of death and manifests as dilated cardiomyopathy (DCM), heart failure, arrhythmias, and sudden death. There is no specific therapy for LMNA-associated cardiomyopathy.

We report that deletion of *Lmna* in cardiac myocytes in mice leads to severe cardiac dysfunction, conduction defect, ventricular arrhythmias, fibrosis, apoptosis, and premature death within 4 weeks. The phenotype is similar to LMNA-associated cardiomyopathy in humans. RNA sequencing, performed prior to the onset of cardiac dysfunction, led to identification of 2,338 differentially expressed genes (DEGs) in *Lmna*-deleted cardiac myocytes. DEGs predicted activation of bromodomain-containing protein 4 (BRD4), a regulator of chromatin-associated proteins and transcription factors, which was confirmed by complementary approaches, including chromatin immunoprecipitation-sequencing. Daily injection of JQ1, a specific BET bromodomain inhibitor partially reversed the DEGs, including those encoding secretome, improved cardiac function, abrogated cardiac arrhythmias, fibrosis, and apoptosis, and prolonged the median survival time by 2-fold in the myocyte-specific *Lmna*-deleted mice. The findings highlight the important role of LMNA in cardiac myocyte and identify BET bromodomain inhibition as a potential therapeutic target in LMNA-associated cardiomyopathy, for which there is no specific effective therapy.

Introduction

Heart Failure is a major cause of morbidity and mortality in the world. (1, 2) It affects an estimated 26 million people worldwide and more than 10% of the elderly in the Western world. (1-3) Prevalence of heart failure continues to rise. An estimated 6.2 million Americans older than 20 years had heart failure between 2013 to 2016 (2.6% of the population) as compared to 5.7 million between 2009-2012. (1) Heart failure remains the number one cause of hospitalization in the United States and Europe. (3)

Dilated cardiomyopathy (DCM), characterized by an increased left ventricular end diastolic diameter (LVEDD) and a reduced left ventricular ejection fraction (LVEF), is a major cause of heart failure and the most common indication for cardiac transplantation. (4-6) DCM is a heterogenous disease with several etiologies. Primary DCM is a genetic disease of the myocardium that typically exhibits an autosomal dominant pattern of inheritance. It is caused primarily by mutations in genes coding for sarcomere and cytoskeletal proteins. (4, 7) Mutations in the *LMNA* gene, encoding nuclear envelope protein lamin A/C (LMNA), are the second most common causes of DCM, accounting for up to 10 % of familial DCM. (8, 9)

Mutations in the *LMNA* gene cause a diverse array of diseases referred to as laminopathies, including DCM, which is a common manifestation. (10-13) DCM caused by *LMNA* mutations (henceforth LMNA-DCM) is the major cause of premature death in laminopathies. (11, 12, 14) LMNA-DCM has a phenotypic expression that is somewhat distinct from DCM caused by mutations in genes encoding sarcomere and cytoskeletal protein, because of a high prevalence of cardiac conduction defects, arrhythmias, and sudden cardiac death (SCD). (8, 9, 11, 14-18) *LMNA* mutations are responsible for about a third of DCM cases associated with cardiac conduction defects. (8) Given the poor prognosis and the high risk of SCD, the presence of *LMNA* pathogenic variants typically necessitates implantation of a defibrillator (11, 12, 15, 18-20).

Despite the clinical significance of LMNA-DCM, there is no specific treatment for this potentially deadly form of heart failure, likely because of our inadequate understanding of its molecular pathogenesis. We and others have recently implicated double-stranded DNA breaks and consequent activation of the DNA damage response (DDR) pathway as an upstream mechanism that instigates induction of phenotype,

comprised of inflammation, apoptosis, cell senescence, fibrosis, cardiac dysfunction, and premature death, in humans and mouse models of LMNA-DCM as well as in other laminopathies. (21-25) Several downstream pathways, including TP53, FOXO3, PDGFRB, and MAPK, are also implicated in the pathogenesis of LMNA-DCM, illustrating complexity of the disease. (13, 26-28)

LMNA is a ubiquitously expressed protein constituent of nuclear inner membrane with low cell type or tissue specificity. (13, 29) However, LMNA interacts with chromatin through Lamin-Associated Domains (LADs) and influences gene expression in a cell type-specific manner. (30-33) In human cardiac myocytes, LMNA interacts with chromatin in about 300 genomic regions, each approximately 2 to 3 million bases in length, and collectively comprise about 20% of the genome. (31) Cell type invariant (constitutive) LADs encompass a minority of the LADs, whereas the majority are facultative and cell type-specific. (30-33) Therefore, cell type-specific interventions in the heart are expected to provide insights into specific role of each cardiac cell type in the pathogenesis of LMNA-DCM and raise the prospect for therapeutic opportunities. Accordingly, we deleted the mouse *Lmna* gene specifically in cardiac myocytes, the main cell type in the heart, characterized the phenotype, and identified the major dysregulated pathways. Deletion of *Lmna* in cardiac myocytes was associated with activation of bromodomain-containing protein 4 (BRD4). Pharmacological targeting of BET bromodomain proteins by JQ1 partially restored dysregulated gene expression, including genes encoding secretome, improved survival, cardiac function, myocardial fibrosis, and apoptosis in the myocyte-specific *Lmna* knock out mouse model of LMNA-DCM. The findings raise the prospect for interventions targeting BET bromodomain proteins for therapeutic gain in LMNA-DCM.

Results

Cardiac myocyte-specific deletion of *Lmna* in mice: *Lmna* gene was deleted in cardiac myocytes by crossing *Lmna*$^{F/F}$ and *Myh6*-Cre deleter mice. (34, 35) Heterozygous and homozygous *Lmna* knock out mice were born per the expected Mendelian ratio and did not show discernible phenotype at birth. To determine efficiency of deletion of the *Lmna* gene in cardiac myocytes, thin myocardial sections from wild type (WT), *Myh6-Cre:Lmna*$^{W/F}$, and *Myh6-Cre:Lmna*$^{F/F}$ mouse hearts were co-stained with antibodies against LMNA and pericentriolar membrane-1 (PCM1), which tags cardiac myocyte nuclei in the heart. (36-38) PCM1 expression was detected in approximately a third of the cells in the myocardium (Figure 1A and B). PCM1 expressing cells also stained positive for expression of LMNA in the WT and *Myh6-Cre:Lmna*$^{W/F}$ mouse hearts (Figure 1A-C). In contrast, only 0.52±0.4% of PCM1 expressing cells, i.e., myocytes, stained positive for LMNA expression in the *Myh6-Cre:Lmna*$^{F/F}$ mouse hearts, indicating a near complete absence of the LMNA protein in cardiac myocytes (Figure 1A-C). To further validate the findings, immunoblotting, using an anti-LMNA antibody, was performed on protein extracts from cardiac myocytes isolated from WT, *Myh6-Cre*:*Lmna*$^{W/F}$, and *Myh6-Cre*:*Lmna*$^{F/F}$ mice. The LMNA protein was reduced in *Myh6-Cre*:*Lmna*$^{W/F}$ and was almost completely absent in the *Myh6-Cre*:*Lmna*$^{F/F}$ myocytes, as compared to WT myocytes (Figure 1D and E). These findings supported efficient deletion of the *Lmna* gene in cardiac myocytes. Expression levels of the LMNA protein in cardiac myocyte extracts from mice carrying the loxP sequences flanking exon 2 of the *Lmna* gene (*Lmna*$^{F/F}$) were similar to those in the WT mice (Supplemental Figure 1, A and B). Likewise, immunoblotting of protein extracts from the non-cardiac myocyte cells in the heart showed unaltered LMNA protein levels in the *Myh6-Cre*:*Lmna*$^{F/F}$ mice (Supplemental Figure 1, C and D).

Gross morphology: *Myh6-Cre*:*Lmna*$^{W/F}$ and *Myh6-Cre*:*Lmna*$^{F/F}$ mice had a normal growth rates for the first 3 weeks of life, but the *Myh6-Cre*:*Lmna*$^{F/F}$ mice showed stunted growth after 3 weeks of life, as indicated by failure to gain weight (Supplemental Figure 2). At 4 weeks of age, the *Myh6-Cre*:*Lmna*$^{F/F}$ mice had a 40.2±2.1% lower body weight as compared to the WT mice. The *Lmna*$^{F/F}$, *Myh6-Cre* and *Myh6-Cre*:*Lmna*$^{W/F}$ mice had a normal growth curve during this period (Supplemental Figure 2).

Survival: The *Myh6-Cre*:*Lmna*$^{F/F}$ mice show increased mortality, notably starting at three weeks of age and rapidly progressing to 100% mortality by 4 weeks (Figure 1F). The *Myh6-Cre*:*Lmna*$^{W/F}$ mice also exhibited an increased mortality albeit at an older age, reaching a 100% mortality by 15 months of age (Figure 1F and inset). The median survival time in *Myh6-Cre*:*Lmna*$^{F/F}$ was 22 days, whereas it was about 8 months in the *Myh6-Cre*:*Lmna*$^{W/F}$ mice (Figure 1F and inset). WT, *Lmna*$^{F/F}$, and *Myh6-Cre* had normal survival (Figure 1F). The survival rates between male and female *Myh6-Cre*:*Lmna*$^{F/F}$ were similar (Supplemental Figure 3).

Cardiac function: The *Myh6-Cre*:*Lmna*$^{F/F}$ mice exhibited cardiac dilatation and systolic dysfunction, as indicated by a markedly increased LVEDD and left ventricular end systolic diameter (LVESD), and reduced LVFS at 3 weeks of age compared to WT mice (Figure 2A; Supplemental Table 1). The heterozygous *Lmna*-deficient mice had a normal cardiac function at 3 weeks of age (Supplemental Table 1). However, these mice developed cardiac dilatation and dysfunction at 10 months of age, the last time point analyzed (Supplemental Table 2). The *Myh6-Cre* and *Lmna*$^{F/F}$ mice, which were included as control, did not show evidence of cardiac dysfunction compared to WT mice (Supplemental Tables 1 and 2). There was no sex-dependent effect on indices of cardiac function in *Myh6-Cre*:*Lmna*$^{F/F}$ mice, as both sexes showed significant cardiac dysfunction at 3 weeks of age (Supplemental Figure 4).

Cardiac arrhythmias: *Myh6-Cre*:*Lmna*$^{W/F}$ and *Myh6-Cre*:*Lmna*$^{F/F}$ mice showed sinus brady-arrhythmias, atrial flutter, atrioventricular blocks (AVB); including complete heart block, ectopic ventricular beats, and ventricular tachycardia (VT), all occurring within the first three weeks in the *Myh6-Cre*:*Lmna*$^{F/F}$ mice and at an older age in the *Myh6-Cre*:*Lmna*$^{W/F}$ mice (Figure 2B, Supplemental Tables 3 and 4). Advanced AVB (2nd and 3rd degree) was common and observed in approximately 2/3rd of the 3-week old *Myh6-Cre*:*Lmna*$^{F/F}$ mice. Likewise, VT (≥ 3 ventricular ectopic beats in the row with a rate of >300 bpm) were recorded in about 20% of the *Myh6-Cre*:*Lmna*$^{F/F}$ mice (Supplemental Table 3). WT, *Lmna*$^{F/F}$ and *Myh6-Cre* mice did not exhibit notable cardiac arrhythmias, except for premature atrial and ventricular contractions (Supplemental Tables 3 and 4).

Myocardial fibrosis and apoptosis: Collagen volume fraction (CVF), a measure of myocardial

fibrosis, was increased by about 8-fold in 3-week old *Myh6-Cre*:*Lmna*$^{F/F}$ as compared to WT mice (Figure 2, C-E). Likewise, the number of TUNEL-positive cells was increased by about 10-fold (Figure 2, F and G).

The heterozygous *Lmna* knock out mice did not exhibit significant myocardial fibrosis or apoptosis at 3 weeks of age but showed increased myocardial fibrosis by 4-fold and apoptosis by ~ 7-fold, as compared to corresponding WT mice at 10 months of age (Supplemental Figure 5). The *Lmna*$^{F/F}$ mice did not show evidence of myocardial fibrosis, as % CVF was similar to that in the WT mice (Supplemental Figure 6).

Differentially expressed genes (DEGs) in cardiac myocytes isolated from *Myh6-Cre*:*Lmna*$^{F/F}$ mouse hearts: To identify transcriptomic changes in cardiac myocytes that are consequent to deletion of the *Lmna* gene but precede the onset of cardiac dysfunction, cardiac phenotype was assessed on 2-week old mice. There was no discernible evidence of cardiac dysfunction on echocardiogram at 2 weeks of age (Supplemental Table 5). Likewise, CVF was not significantly different between the WT and *Myh6-Cre*:*Lmna*$^{F/F}$ mice and the number of TUNEL positive cells was also similar between the two genotypes (Supplemental Figure 7). Therefore, cardiac myocytes were isolated from 2-week old WT and *Myh6-Cre*:*Lmna*$^{F/F}$ mice to extract RNA for RNA sequencing (RNA-Seq).

Principal Component Analysis of the RNA-Seq data showed segregation of the samples according to the mouse genotype (Supplemental Figure 8). A total of 2,338 genes were differentially expressed in the *Myh6-Cre*:*Lmna*$^{F/F}$ as compared to WT cardiac myocytes, of which 1,419 genes were downregulated whereas transcript levels of 919 genes were increased (Figure 3A). Unsupervised hierarchical clustering showed distinct grouping of the samples per genotypes (Figure 3B).

Ingenuity Pathway Analysis (IPA) of DEGs predicted activation of transcriptional regulators lysine demethylase 5A (KDM5A), TP53, mitogen-activated protein kinase 4 (MAP4K4), nuclear receptor interacting protein 1 (NRIP1), BRD4, and ERG1 in the *Myh6-Cre*:*Lmna*$^{F/F}$ mouse cardiac myocytes (Figure 3C). In contrast, retinoblastoma 1 (RB1), insulin receptor (INSR) and peroxisome proliferator activated receptor gamma coactivator 1α (PPARGC1α) were predicted to be suppressed (Figure 3D).

Gene Set Enrichment Analysis (GSEA) of DEGs against Hallmark Molecular Signature Database identified enrichment for genes involved in epithelial to mesenchymal transition (EMT), inflammation, and apoptosis (Figure 3E), whereas genes involved in oxidative phosphorylation, metabolism, and myogenesis were under-represented (Figure 3F).

The DEGs were analyzed to identify genes whose protein products are known or expected to be secreted, i.e., the secretome. A total of 168/2,338 (7.2%) DEGs coded for secretome, which are depicted in a heat map in Supplemental Figure 9A. To validate the RNA-Seq data, RT-qPCR was performed, which showed changes concordant with the RNA-Seq findings for 17/18 (13 increased and 4 decreased) genes tested and one gene was unchanged (Supplemental Figure 9, B and C). DEGs coding for secretome predicted TGFβ1 as the most activated and α-catenin as the most suppressed regulators of gene expression (Figure 9D). GSEA plot showing enrichment of genes in the TGFβ1 pathway is illustrated in Supplemental Figure 9E. Immunoblotting of cardiac myocyte extracts suggested increased levels of the active TGFβ1 protein in the *Myh6-Cre*:*Lmna*$^{F/F}$ cardiac myocytes (Supplemental Figures 9F and G). In accord with activation of TGFβ1, the differentially expressed genes encoding secretome were involved in EMT, angiogenesis, STAT signaling, hypoxia, and apoptosis (Supplemental Figure 9H).

Activation of BRD4 in *Myh6-Cre*:*Lmna*$^{F/F}$ cardiac myocytes: Predicted activation of BRD4 based on the DEGs was in accord with activation of EMT in the heart and the prominent expression of myocardial fibrosis in *Myh6-Cre*:*Lmna*$^{F/F}$ hearts, rendering BRD4 as a potential therapeutic target. To strengthen the evidence for activation of BRD4, DEGs in the *Myh6-Cre*:*Lmna*$^{F/F}$ cardiac myocytes were analyzed against three publicly available mouse heart and one rat cardiac myocyte RNA-Seq datasets with defined BRD4 targets. (39-41) BRD4 targets in each dataset were defined as genes whose transcript levels were increased in the pathological state (including intervention) but were reduced subsequently upon inhibition of BRDs or BRD4. As shown in the GSEA plots in Figure 4A, BRD4 target genes, identified in four publicly available datasets, were enriched in *Myh6-Cre:Lmna*$^{F/F}$ cardiac myocytes. Similarly, DEGs in *Myh6-Cre:Lmna*$^{F/F}$ cardiac myocytes were also enriched for the BRD4 target genes gathered from the IPA

datasets (Figure 4B). Transcript levels of the BRD4 target genes, identified in all four datasets and from IPA database, in the *Myh6-Cre:Lmna*$^{F/F}$ cardiac myocytes are depicted in a heat map (Figure 4C). As shown, transcript levels of 123 BRD4 target genes were upregulated in the *Myh6-Cre:Lmna*$^{F/F}$ cardiac myocytes as compared to WT myocytes, whereas expression of 17 genes were suppressed (p<0.0001, Figure 4C).

To determine whether increased transcript levels of BRD4 was because of increased BRD4 protein levels, immunoblotting was performed on cardiac myocyte protein extracts from the WT and *Myh6-Cre:Lmna*$^{F/F}$ mice. There was no difference in the BRD4 protein levels between the two groups (Supplemental Figure 10). Likewise, BRD2 and BRD3 protein levels were unchanged (Supplemental Figure 10).

BRD4 ChIP-Seq: To determine whether increased transcript levels of BRD4 target genes in the *Myh6-Cre*:*Lmna*$^{F/F}$ cardiac myocytes were because of increased recruitment of the BRD4 to the chromatin, BRD4 ChIP-Seq was performed on myocyte chromatin extracts using an anti-BRD4 antibody. Representative IVG tracks showing BRD4 enrichment in the corresponding regions in the *Myh6-Cre*:*Lmna*$^{F/F}$ myocytes are shown (Figure 5A). The total number of peaks in each ChIP-Seq experiment and the intersects showing shared peaks between the samples in each genotype are presented in the Venn diagrams in Supplemental Figure 11A. BRD4 ChIP peaks were redistributed in the *Myh6-Cre*:*Lmna*$^{F/F}$ as compared to WT cardiac myocyte genomes, as only about 10,776/44,947 (24%) of the peaks were shared between the two genotypes (Supplemental Figure 11B). Approximately 6,000 BRD4-enriched peaks were overlapped in at least two genomes in the WT or *Myh6-Cre:Lmna*$^{F/F}$ myocytes, of which 758 (12.6%) were exclusive to WT, and 1,946 (32.4%) to *Myh6-Cre:Lmna*$^{F/F}$ genomes (Supplemental Figure 11C). Distributions of BRD4 ChIP-Seq peaks differed for their localizations to genomic partitions between the WT and *Myh6-Cre:Lmna*$^{F/F}$ myocytes, as more peaks were located in the upstream (p=0.0007) and downstream (p<0.0001) genomic regions in the *Myh6-Cre:Lmna*$^{F/F}$ genomes (Supplemental Figure 11D).

To validate the BRD4 ChIP-Seq findings, ChIP was performed on an independent set of chromatin extracts from the WT and *Myh6-Cre:Lmna*$^{F/F}$ myocytes. The chromatin precipitates were analyzed for the enrichment of the genomic DNA mapped to the peak regions in the discovery ChIP-Seq experiments. As

shown in Figure 5, A and B, genomic DNA located at the BRD4 ChIP-Seq peaks were enriched both in the WT and *Myh6-Cre:Lmna*$^{F/F}$ myocytes in the independent validation ChIP experiments, albeit the enrichment was greater in the *Myh6-Cre:Lmna*$^{F/F}$ than in the WT myocytes.

To determine whether recruitment of BRD4 to chromatin affected gene expression in the *Myh6-Cre:Lmna*$^{F/F}$ myocytes, transcript levels of the annotated genes located in the BRD4 peak and outside of the peak regions were compared. Globally, transcript levels of genes located at the peak regions were higher as compared to those located outside of the peak regions (Figure 5C). Representative genome browser tracks of the transcript levels at the peak regions as compared to regions outside of peaks are shown in Supplemental Figure 12A. Likewise, gain-of-peak (GoP), defined as peak present in the *Myh6-Cre:Lmna*$^{F/F}$ and absent in the WT, was associated with a greater number of genes (a higher gene density) that were upregulated, as compared to loss-of-peak (LoP), defined as peaks absent in the *Myh6-Cre:Lmna*$^{F/F}$ but present in the WT myocytes (Supplemental Figure 12B). Likewise, a greater number of DEGs located at the GoP regions were upregulated as compared to DEGs located at the LoP regions (Figure 5C and Supplemental Figure 12B). The difference in the gene density was also remarkable for the upregulated DEGs located at the upstream genomic regions (Supplemental Figure 12C).

Given the differences in genomic partition of BRD4 peaks, distribution of the annotated DEGs in each genomic segment was compared between the WT and *Myh6-Cre:Lmna*$^{F/F}$ myocytes (Supplemental Figure 12D). Only distribution of DEGs located in the upstream genomic regions differed significantly between the WT and *Myh6-Cre:Lmna*$^{F/F}$ myocytes (Supplemental Figure 12D). Finally, LoP in the *Myh6-Cre:Lmna*$^{F/F}$ genome was associated with a larger number of DEGs located in the upstream region (39/54 (72%) whose expression levels were suppressed (Supplemental Figure 12E).

Dose titration studies with JQ1: Given the data indicating activation of BDR4 in the *Myh6-Cre:Lmna*$^{F/F}$ myocytes, phenotypic effects of pharmacological BET bromodomain inhibition were analyzed in the *Myh6-Cre*:*Lmna*$^{F/F}$ mice. The primary end point was survival and the secondary end points were myocardial function and fibrosis. The latter was selected based on evidence of enrichment of the DEGs for EMT, presence of myocardial fibrosis in *Myh6-Cre*:*Lmna*$^{F/F}$ hearts, and the prominent anti-fibrotic effects

of BRD4. (41-43)

JQ1, a well-established specific pan-inhibitor of BET bromodomain proteins was selected to treat the *Myh6-Cre*:*Lmna*$^{F/F}$ mice. (44) The life span of the *Myh6-Cre*:*Lmna*$^{F/F}$ mice being ~ 3 to 4 weeks necessitated administration of JQ1 at a very young age, which was counterbalanced by potential fortuitous effects arising because of the prominent role of epigenetic regulation during cardiac development and myocyte maturation/proliferation in early post-natal stage. (45-47) Consequently, a series of time course studies were performed in the WT mice to determine the effects of injection of JQ1 at the commonly used dose of 50 mg/Kg/day of JQ1 at post-natal day 4, 7, 10, and 14 on survival and body growth. (42, 44) JQ1 administration at 50 mg/Kg/day was associated with increased mortality, growth retardation, and alopecia at the injection site, which were more pronounced when injected at earlier than later time points (Supplemental Figure 13). Injection of JQ1 at a later time point (after P14) was not considered because of the potential confounding effects of early mortality of the *Myh6-Cre*:*Lmna*$^{F/F}$ mice. Therefore, JQ1 dose was reduced to 20 mg/Kg/day, which has been shown to effectively inhibit BET bromodomain protein activity. (48, 49) JQ1 administered at 20 mg/Kg/day did not affect survival or gain-in-weight in the WT mice (Supplemental Figure 14). Consequently, the subsequent experiments in WT and *Myh6-Cre*:*Lmna*$^{F/F}$ mice were performed with 20 mg/Kg/d injected subcutaneously beginning at P14.

Effects of JQ1 on cardiac myocyte transcripts and regulatory pathway: RNA was extracted from cardiac myocytes isolated from 3-week old WT, *Myh6-Cre:Lmna*$^{F/F}$ treated with a vehicle, and *Myh6-Cre:Lmna*$^{F/F}$ mice treated with JQ1 (20 mg/Kg/day) for one week (P14 to P21). Gene expression was analyzed by RNA-Seq. Treatment with JQ1 shifted transcriptomic profile of the cardiac myocytes toward that of the WT, as illustrated in the heat map (Figure 6A). Overall, a total of 1,817 genes were differentially expressed between the WT and *Myh6-Cre:Lmna*$^{F/F}$ myocytes. Treatment with JQ1 normalized transcript levels of 152 genes (no difference between JQ1 treated *Myh6-Cre:Lmna*$^{F/F}$ and WT myocytes) and significantly lowered transcript levels of another 410 genes (Figure 6B). Overall, transcript levels of 562 DEGs (31%) had reversed toward normal (Figure 6B). To determine efficacy of treatment with JQ1 on suppressing BRD4 activity, transcript levels of the BRD4 target genes in the untreated and JQ1-treated

Myh6-Cre:Lmna$^{F/F}$ myocytes were compared. GSEA showed suppression of the BRD4 target gene transcript levels in the JQ1 treated myocytes as compared to untreated *Myh6-Cre:Lmna*$^{F/F}$ myocytes (Figure 6, C and D).

To validate the RNA-Seq data, transcript levels of 32 BRD4 target genes were quantified by RT-qPCR in cardiac myocyte RNA extracts from the WT, *Myh6-Cre:Lmna*$^{F/F}$ treated with a vehicle (10% DMSO and 10% 2-Hydroxypropyl-β-cyclodextrin), and *Myh6-Cre:Lmna*$^{F/F}$ treated JQ1 treated (20 mg/Kg/d for 7 days, starting at P14). Treatment with JQ1 normalized elevated transcript levels of 15/30 selected BRD4 target genes and significantly reduced, but not normalized, levels of another 7 target genes (Figure 6E and Supplemental Figure 15A). JQ1 treatment did no effect on transcript levels of 9 selected DEGs, whereas transcript level of one candidate target gene was similar among the three groups. i.e., not differentially expressed (Supplemental Figure 15B).

Genes whose transcript levels were significantly affected by JQ1 treatment were analyzed by IPA to infer the transcriptional regulators. The approach predicted activation of over a dozen regulators of gene expression, including TGFβ1, STAT1, and RELA among others (Figure 7, A and B) A complete list of dysregulated growth/paracrine factors and transcriptional regulators is provided in Supplemental Table 6. Biologically, genes regulated by JQ1 were involved in EMT and innate immune response, among others (Figure 7C). Concordant with this finding, GSEA showed activation of the EMT pathway in *Myh6-Cre:Lmna*$^{F/F}$ and its reversal upon treatment with JQ1 (Figure 7D and E).

The RNA-Seq data were also analyzed for the effects of treatment with JQ1 on expression levels of genes encoding secreted proteins (secretome). Treatment with JQ1 shifted the secretome profile of the *Myh6-Cre:Lmna*$^{F/F}$ toward that of the WT myocytes, involving 195 genes, as depicted in the heat map shown in Supplemental Figure 16A. Treatment with JQ1 normalized transcript levels of 21 genes encoding secretome and significantly reduced transcript levels of another 50 genes, albeit the latter group was not normalized (Supplemental Figure 16B). The findings were tested for validation by RT-qPCR, which were in agreement with the RNA-Seq data, as transcript levels of 11/12 (92%) upregulated genes were either normalized or partially reduced (Supplemental Figure 16C). Analysis of the DEGs encoding secretome

predicted activation of several growth and paracrine factors, including GDF15, TGFβ1, and FGF21 among others, which might contribute to the pathogenesis of the phenotype (Supplemental Figure 16D). The findings of a similar analysis to predict transcriptional regulators of secretome is presented in Supplemental Figure 16E. Finally, genes encoding secretome were mostly involved in extracellular matrix formation and deposit (Supplemental Figure 16F).

Effects of JQ1 on survival: To determine effects of treatment with JQ1 on survival, WT and *Myh6-Cre*:*Lmna*$^{F/F}$ mice were treated with daily subcutaneous injection of either a vehicle (10% DMSO and 10% 2-Hydroxypropyl-β-cyclodextrin) or JQ1 (20mg/Kg/d) starting at P14. A group of untreated littermate mice were included as a control. Treatment with JQ1 prolonged median survival of the *Myh6-Cre*:*Lmna*$^{F/F}$ mice from 23 days to 32 days and the maximum life span from 28 to 42 days (X^2=126.1, p<0.0001, Figure 8A). There were no differences in the survival rates between untreated or *Myh6-Cre*:*Lmna*$^{F/F}$ mice treated with the vehicle (X^2=1.69, p=0.19). Likewise, treatment with JQ1 had no effect on the survival rate of the WT mice.

Effects of JQ1 on body weight: Treatment with JQ1 had no discernible effect on body weight in the *Myh6-Cre*:*Lmna*$^{F/F}$ or WT mice (Supplemental Figure17). *Myh6-Cre*:*Lmna*$^{F/F}$ mice, regardless of the treatment groups, had a smaller body weight after 3 weeks of age as compared to the WT mice.

Effects of JQ1 on cardiac function: WT and *Myh6-Cre*:*Lmna*$^{F/F}$ mice were treated with a vehicle or JQ1 at 20 mg/Kg/d starting at P14 and cardiac size and function were assessed by echocardiography at 3 weeks of age. Treatment with JQ1 improved left ventricular size and function in the *Myh6-Cre*:*Lmna*$^{F/F}$ mice, as indicated by a smaller LVEDD and LVESD, improved LVFS, and reduced left ventricular mass (Table 1 and Figure 8B). Genotype-by-treatment interaction analysis showed significant effects of the genotype alone, treatment alone, and genotype-by-treatment interactions on the LVFS (Table 1). Treatment with JQ1 did not have a discernible effect on echocardiographic indices of cardiac size and function in the WT mice (Table 1).

Effects of JQ1 on molecular markers of cardiac dysfunction: Cardiac hypertrophy and failure are associated with changes in expression of a number of genes referred to as markers of cardiac

hypertrophy and dysfunction, including *Nppa*, *Nppb*, *Myh6*, *Myh7*, *Atp2a2*, and *Actc1*. (50-52) To corroborate the beneficial effects of JQ1 on survival and cardiac function, transcript levels of the molecular markers of cardiac dysfunction were quantified by RT-qPCR on cardiac RNA extracts. Transcript levels of *Nppa*, *Nppb*, *Myh7*, and *Actc1* were increased and those of *Atp2a2* and *Myh6* were reduced in the *Myh6-Cre*:*Lmna*$^{F/F}$ hearts, which were in accord with the anticipated changes in cardiac hypertrophy and failure. (50-52) Treatment with JQ1 completely or partially rescued transcript levels of the molecular markers of cardiac hypertrophy and dysfunction (Figure 8C).

Effects of JQ1 on cardiac arrhythmias: Phenotypic characteristics of human LMNA-DCM includes conduction defects and ventricular arrhythmias, which were also observed in the *Myh6-Cre*:*Lmna*$^{F/F}$ mice (Figure 2B, Supplemental Table 3). Treatment with JQ1 significantly reduced frequency of supraventricular arrhythmias, AV blocks, and ventricular arrhythmias, the findings which were in accord with improved survival in the JQ1 treated *Myh6-Cre*:*Lmna*$^{F/F}$ mice (Supplemental Table 7)

Effects of JQ1 on myocardial fibrosis: Given the marked dysregulation of EMT signature in the *Myh6-Cre*:*Lmna*$^{F/F}$ cardiac myocytes and in view of the well-established effects of BRD4 in mediating fibrosis in various organs, effects of JQ1 administration on myocardial fibrosis was assessed by determining CVF and transcript levels of genes involved in fibrosis. (40, 42) CVF comprised 8.3±2.6 and 6.6±0.9% of the myocardial area in the untreated and vehicle-treated *Myh6-Cre*:*Lmna*$^{F/F}$ mice, respectively (p<0.01 compared to WT, Figure 9, A-C). Treatment with JQ1 reduced CVF by about 68% (p<0.0001) as compared to WT and by ~ 60% (p=0.013) as compared to vehicle treated *Myh6-Cre*:*Lmna*$^{F/F}$ mice (Figure 9, A-B). Consequently, CVF in JQ1 treated *Myh6-Cre*:*Lmna*$^{F/F}$ mice was similar to that in the WT mice.

To corroborate the findings, transcript levels of 13 genes involved in myocardial fibrosis were quantified by RT-qPCR on whole heart RNA extracts. As shown in Figure 9D, treatment with JQ1 normalized or reduced transcript levels of 12/13 (92%) genes in the *Myh6-Cre*:*Lmna*$^{F/F}$ mouse hearts (Figure 9D). Among genes analyzed only transcript levels of *Col6a3* were not different among four experimental groups (Figure 9D).

Effects of JQ1 on myocardial apoptosis: Given increased apoptosis in the myocardium of *Myh6-*

Cre:*Lmna*$^{F/F}$ mice, effect of treatment with JQ1 on myocardial apoptosis was assessed by TUNEL assay and transcript levels of the molecular markers of apoptosis. The number of TUNEL-positive cells was increased markedly (~ 7-fold) in the myocardium of *Myh6-Cre*:*Lmna*$^{F/F}$ mice at 3 weeks of age (Figure 10, A and B). Treatment with JQ1 was associated with a 50% reduction in the number of TUNEL-positive cells in the myocardium of *Myh6-Cre*:*Lmna*$^{F/F}$ mice as compared to untreated or vehicle-treated mice (p<0.009 and p<0.002, respectively).

To corroborate the findings, transcript levels of 9 markers of apoptosis were quantified by RT-qPCR on whole heart RNA extracts in the experimental groups. Transcript levels of *Bcl2*, *Bnip3, Bbc2,* and *Bcl2l1* were fully rescued (not different from the WT) whereas that of *Gadd45b* remained increased in the myocardium of *Myh6-Cre*:*Lmna*$^{F/F}$ (Figure 10C). Transcript levels of *Gadd45a* and *Tnfsf10,* which were reduced in the *Myh6-Cre*:*Lmna*$^{F/F}$ myocardium, did not change upon treatment with JQ1 (Figure 8C). Finally, treatment with JQ1 had no significant effect on transcript levels of *Gadd45g* and *Bax*, which were unaltered in the myocardium of *Myh6-Cre*:*Lmna*$^{F/F}$ mice (Figure 10C).

Discussion

We report that genetic deletion of the *Lmna* gene exclusively in cardiac myocytes led to a dose-dependent cardiac dilatation and dysfunction, cardiac arrhythmias; including conduction defects and ventricular arrhythmias, myocardial fibrosis, and apoptosis, and resulted in total mortality within 4 weeks in the homozygous, and 15 months in the heterozygous mice. Transcriptomic analysis identified dysregulation of a dozen transcriptional regulators, including the epigenetic reader BRD4, which was activated in the *Lmna* null cardiac myocytes. Treatment of *Lmna* deficient mice with JQ1, a well-characterized and specific inhibitor of the BET bromodomain proteins, prolonged survival and improved cardiac function, cardiac arrhythmias, myocardial fibrosis, and apoptosis. (44) These findings in a genetically defined mouse model of LMNA-DCM set the stage for advancing the findings on beneficial effects of inhibition of BRD4 towards treatment of human patients with DCM in laminopathies.

Because LMNA is a ubiquitously expressed protein, mutations in the *LMNA* gene are expected to affect multiple cell types. (13, 29) The ensuing clinical phenotype associated with the *LMNA* mutations is

the consequence of changes in multiple cell types. Deletion of the *Lmna* gene exclusively in cardiac myocytes recapitulated several components of LMNA-associated DCM in humans, including cardiac dysfunction, arrhythmias, fibrosis, and apoptosis. The cardiac phenotype in the *Myh6-Cre:Lmna*$^{F/F}$ mice is not distinct from that observed in mice with systemic deletion of *Lmna* or expressing LMNA with missense mutations, but perhaps is more pronounced. (28, 53, 54) The similarities in the findings between the myocyte-specific and systemic deletion of the *Lmna* gene, signify the crucial role of cardiac myocytes in cardiomyopathies resulting from mutations in the *LMNA* gene. However, the beneficial effects of treatment with JQ1 might be in part mediated through the effects on systemic delivery of JQ1 on other cardiac cell types, in addition to its effects on cardiac myocytes.

BRD4 was among the top dysregulated epigenetic factors in *Myh6-Cre*:*Lmna*$^{F/F}$ myocytes, whose major function is to promote transcription by binding to acetylated histones, transcription factors, and other chromatin-associated proteins, resulting in recruitment of positive regulators of gene expression and displacement of the negative regulators. (55) Consistent with this knowledge, transcript levels of 123/145 (85%) of BRD4 target genes, collected from four public datasets and IPA, were increased in *Myh6-Cre*:*Lmna*$^{F/F}$ myocytes. Furthermore, ChIP-Seq data showed enriched recruitment of BRD4 and overall an increased expression of genes associated with these BRD4 peaks in the *Myh6-Cre*:*Lmna*$^{F/F}$ myocytes, which provided further evidence in support of activation of BRD4-mediated transcription. Consequently, multiple lines of evidence of activation of BRD4 in cardiac myocytes set the rationale for pharmacological inhibition of BRD4 in *Myh6-Cre*:*Lmna*$^{F/F}$ myocytes. The approach was also in accord with the prominent phenotype of myocardial fibrosis in the *Myh6-Cre*:*Lmna*$^{F/F}$ mice and the well-established role of BRD4 in EMT, as well as the emerging role of inhibitors of BRD4 in reversing fibrosis and attenuating myocardial dysfunction. (39-42)

The beneficial effects of treatment with JQ1 were concordant across multiple phenotypes, including prolonged survival, reduced cardiac conduction defects and arrhythmias, and improved cardiac function, fibrosis, and apoptosis, which were corroborated by complementary methods, whenever applicable. Likewise, administration of JQ1 partially restored dysregulated cardiac myocyte transcriptome, particularly

transcripts of the genes involved in inflammation and those encoding cardiac secretome and their upstream regulators, such as the TGFβ1 pathway. Partial restoration of secretome was associated with attenuation of EMT and myocardial fibrosis. Similarly, administration of JQ1 attenuated myocardial apoptosis, which is likely a phenotype effect of the secretome, however, the identity of myocardial cell undergoing apoptosis in the *Myh6-Cre:Lmna*$^{F/F}$ hearts could not be ascertained by the TUNEL assay. Improvement of cardiac function was likely the consequence of effects of JQ1 on myocytes, including secretome, as well as its effects on non-myocyte cells. The rescue while remarkable for the relatively large effect sizes on all assessed phenotypes, was incomplete. Treatment with JQ1 delayed premature death, improved cardiac function and reduced arrhythmias, but did not fully abrogate the LMNA-DCM phenotype. The incomplete rescue likely had multiple reasons, including multifarity of the pathways involved in the pathogenesis of LMNA-DCM, such as activation of KDM5A, MAP4K4, and TP53 as well as suppression of RB1 and INSR transcriptional regulators, among others, as well as the study design pertaining to dose, timing, and route of administration of JQ1. Several of the upstream regulatory pathways predicted to be dysregulated in the *Myh6-Cre:Lmna*$^{F/F}$ myocytes, including TP53, have been previously implicated in the pathogenesis of LMNA-associated DCM in humans and mouse models. (21, 28) However, administration of JQ1 only rescues a fraction of the dysregulated pathways and a few of them only partially, which in part may explain incomplete phenotypic rescue. The complexity of the LMNA-DCM phenotype would necessitate targeting of multiple pathogenic pathways for a superior therapeutic gain. This notion is in accord with the current therapeutic practice in treatment of complex phenotypes, such as heart failure, wherein the effect size of each therapeutic modality, while significant, is relatively modest, necessitating poly pharmacy.

The findings in LMNA-DCM mice are in agreement with the previous data on the pro-fibrotic effects of BRD4 and the beneficial effects of JQ1, a first-in-class pan-inhibitor of BET bromodomain proteins, on attenuating myocardial fibrosis and cardiac dysfunction in pressure overload and myocardial infarction mouse models. (39, 41) Suppression of cardiac arrhythmias upon treatment with JQ1 is remarkable and a novel finding. Several mechanisms are likely to be involved in the beneficial effects of JQ1 in heart failure and pro-fibrotic conditions. The core mechanism likely pertains to competitive

displacement of BRD proteins by JQ1 from acetyl-lysine recognition motif on histones, and the consequent suppression of aberrant gene expression. (44)

The molecular mechanism(s) responsible for activation of BRD4 in *Myh6-Cre*:*Lmna*$^{F/F}$ mouse heart is unknown. Co-immunoprecipitation studies do not show an interaction between the LMNA and BRD4 proteins. In addition, transcript levels of *Brd4* were not significantly changed in *Myh6-Cre*:*Lmna*$^{F/F}$ myocytes, suggesting a post-transcriptional mechanism(s) for activation of BRD4, such as hyperphosphorylation, which is typically mediated by CDK9. (56) Previous data suggest that activation of BRD4 in cardiac fibroblasts is mediated, in part, through P38 MAP kinase (MAPK14) and TGFβ1 pathways. (42) The activation leads to recruitment of BRD4 to enhancers provoking expression of pro-inflammatory and pro-fibrotic genes through yet-to-be-defined mechanism(s). (42) It is noteworthy that TGFβ1 and MAP4K4, the latter known to regulate p38, were amongst the top activated transcriptional co-regulator in *Myh6-Cre*:*Lmna*$^{F/F}$ myocytes (Figure 3C). (57, 58) Several alternative mechanisms might also be involved, such as chromatin conformational and epigenetic changes in the absence of LMNA, which might lead to activation of BRD4 in cardiac myocytes.

The findings showing beneficial effects of treatment with JQ1 in the *Myh6-Cre*:*Lmna*$^{F/F}$ mice serve as the proof-of-principle data, which set the stage for additional pre-clinical studies in heterozygous *Lmna* knock out mice, and pilot clinical studies in humans to advance utilities of targeting BRD4 in LMNA-DCM. Given the paucity of specific therapies for LMNA-DCM, inhibition of BET bromodomain, with specific and relatively safe drugs, could emerge as an effective therapy that targets a specific pathogenic pathway in LMNA-DCM.

Methods

Detailed Material and Methods Section is provided as Supplementary Material.

Mouse models: *Myh6-Cre, Myh6-Cre:Lmna*$^{W/F}$, and *Myh6-Cre:Lmna*$^{F/F}$ mice were generated per conventional methods. (34, 35) Oligonucleotide primers used in PCR reactions are listed in Table S7.

Survival: Survival was analyzed by constructing Kaplan-Meier survival plots.

Echocardiography and Electrocardiography (EKG): Cardiac size and function were assessed in age- and sex-matched mice at 2 weeks, 3 weeks and 10 months of age by echocardiography, as published. (21, 28, 59) Indices of cardiac size and function were measured in 5-6 cardiac cycles. Left ventricular fractional shortening and mass were calculated from the measured indices.

Surface ECG was obtained by placing needle-electrodes subcutaneously and connecting them to an ECG recording unit.

Isolation of cardiac myocytes: Cardiac myocytes were isolated by collagenase perfusion of the myocardium, as published. (28)

Histology: Myocardial fibrosis was quantified by determining CVF in myocardial sections as published. (28, 59, 60)

Immunoblotting and immunofluorescence: Expression levels of the proteins of interest were detected and quantified by immunoblotting, as published. (21, 59) Immunofluorescence was performed to detect expression and localization of LMNA and PCM1 proteins, using specific antibodies, as published. (21, 59, 60) A detailed list of antibodies used is provided in Table S7.

Detection of apoptosis: Apoptosis was detected by nick-end labeling of DNA with the TUNEL assay, as described. (21, 59, 60) Percentage of TUNEL-positive nuclei was determined in 6,400 to 16,500 DAPI-positive nuclei per mouse.

Quantitative real-time PCR (RT-qPCR): Transcript levels of selected genes were determined by RT-qPCR using specific TaqMan gene expression assays or SYBR Green specific primers, and normalized to glyceraldehyde-3-phosphate dehydrogenase (*Gapdh*) mRNA levels, as published. (21, 59) Taqman probes and SYBR Green primers are detailed in Table S7.

RNA-Sequencing (RNA-Seq): RNA-seq was performed on ribosome-depleted RNA extracted from the heart of 2-week old WT and *Myh6-Cre:Lmna*$^{F/F}$ as well as in 3-week old WT, vehicle-treated, and JQ1-treated mice, as published. (21, 59, 60) Samples with an RNA Integrity Number (RIN) readout of more than 8 were used for library preparation and sequencing to generate 75 or 100 base pair runs. DEGs were identified using the edgeR, voom, and DESeq2, following RUV (Removed Unwanted Variation) adjustment and annotated using the GENCODE gene model (https://www.gencodegenes.org/mouse/). (61-64) Pathway analysis was performed by Gene Set Enrichment Analysis (GSEA, version 2.2.3, http://software.broadinstitute.org/gsea/) using the ranked gene list. (65) Activation of BRD4 was further validated against BRD4 target genes reported in 4 independent public datasets. (39, 41) Differentially expressed genes encoding the secreted proteins were obtained as published.(59)

ChIP-Seq: Myocytes were isolated and chromatin was cross-linked with 1% formaldehyde, nuclei were extracted and homogenized in a nuclear lysis buffer, and chromatin was sheared by sonication, as published. (31) After overnight immunoprecipitation with an anti-BRD4 antibody, the complexes were immunoprecipitated. The chromatin elution was treated with RNAse A and proteinase K, and the DNA was extracted using phenol/chloroform and ethanol precipitation. The protocol was also followed for the DNA sample used for sequencing as well as ChIP-PCR. Libraries were prepared and single read of 50 bp length were sequenced.

Sequencing of BRD4 ChIP-Seq libraries yielded 36-65 million single-end reads. Reads were aligned to the mouse genome (mm10 release) by Bowtie v 2.3.4.3 and uniquely mapping reads were analyzed. ChIP-seq peaks were called using MACS2 from Galaxy (Version 2.1.1). (66) Enriched regions were intersected using tools Multiple Intersect (Galaxy Version 2.27.1) and regions present in at least two

samples per genotype were considered as BRD4-bound regions (q<0.05). BRD4 bound regions that were present in the *Myh6-Cre:Lmna*$^{F/F}$ but absent in the WT samples were considered as Gain of Peak (GoP) and those that were unique to WT as Loss of Peak (LoP). Plots showing gene density vs expression were generated using the density plots and the sort map function in R (https://cran.r-project.org/) and EaSeq (http://easeq.net. (67) Data was deposited in GEO (GSE142129). ChIP-seq signal and genomic localization were visualized using Integrative Genomics Viewer (IGV). Genomic location showing BRD4 enrichment at its putative targets were obtained from IGV.

ChIP-qPCR: The ChIP-Seq findings were tested for validation in an independent set of ChIP experiment using an anti-BRD4 antibody on cardiac myocyte chromatin extracted from the WT and *Mhy6-cre:Lmna*$^{F/F}$ mice, as described above. Genomic regions showing enrichment for the BRD4 recruitment were visualized using The Integrative Genomics Viewer (IGV). (68) The sequence flanking the enriched regions were used to design oligonucleotide primers and qPCR was performed to determine enrichment of the BRD4 recruitment in the WT and *Mhy6-cre:Lmna*$^{F/F}$ samples.

Statistics: Normality of data distribution was assessed by Shapiro-Wilk's test. Data that followed a Gaussian distribution pattern were presented as mean ± SD and compared using unpaired t-test, ordinary One-Way ANOVA, or two-way ANOVA, followed with Tukey or Bonferroni multiple comparison test, as appropriate. Otherwise, data were presented as the median values and compared by Kolmogorov-Smirnov, Kruskal-Wallis, or Mann-Whitney test followed with Dunn's test correction for multiple comparison. Survival rates were analyzed by constructing Kaplan-Meier survival plots and comparing the survival rate by Log-rank (Mantel-Cox) test. A q value of <0.05 and a p value of <0.05 were considered significant.

Institutional approval: The animal care and use committee of the University of Texas Health Science Center approved the mouse studies.

Author contributions:

Gaelle Auguste: Performed most of the molecular biology and genomic experiments, including preparation of samples for RNA-Seq and ChIP-Seq; performed echocardiography, and electrocardiographic rhythm monitoring; analyzed the data, and drafted as well as edited the manuscript.

Leila Rouhi: Performed part of the RT-qPCR, ChIP-qPCR experiments, and immunoblotting.

Scot J Matkovich: Performed bioinformatics analysis of RNA-Seq data

Cristian Coarfa: Performed bioinformatics analysis of RNA-Seq and ChIP-Seq data

Matthew J. Robertson: Performed bioinformatics analysis of RNA-Seq data

Grazyna Czernuszewicz: Assisted in mice genotyping

Priyatansh Gurha: Analyzed the RNA-Seq and ChIP-Seq data and edited the manuscript

Ali J. Marian: Developed the concept, supervised the experiments, interpreted the findings, and wrote the manuscript

Acknowledgments: This work was supported in part by grants from NIH, National Heart, Lung and Blood Institute (NHLBI R01 HL088498, 1R01HL132401, R01HL151737, and S10 OD018135), Leducq Foundation (14 CVD 03), NIA (R21 AG060413-01), The American Heart Association (19POST34410032), The Ewing Halsell Foundation, George and Mary Josephine Hamman Foundation, TexGen Fund from Greater Houston Community Foundation.

REFERENCES

1. Benjamin EJ, Muntner P, Alonso A, Bittencourt MS, Callaway CW, Carson AP, et al. Heart Disease and Stroke Statistics-2019 Update: A Report From the American Heart Association. *Circulation.* 2019;139(10):e56-e528.
2. Savarese G, and Lund LH. Global Public Health Burden of Heart Failure. *Card Fail Rev.* 2017;3(1):7-11.
3. Ambrosy AP, Fonarow GC, Butler J, Chioncel O, Greene SJ, Vaduganathan M, et al. The global health and economic burden of hospitalizations for heart failure: lessons learned from hospitalized heart failure registries. *J Am Coll Cardiol.* 2014;63(12):1123-33.
4. McNally EM, Mestroni, Luisa. Dilated Cardiomyopathy: Genetic determinants and mechanisms *Circulation Research.* 2017.
5. Metra M, Ponikowski P, Dickstein K, McMurray JJ, Gavazzi A, Bergh CH, et al. Advanced chronic heart failure: A position statement from the Study Group on Advanced Heart Failure of the Heart Failure Association of the European Society of Cardiology. *Eur J Heart Fail.* 2007;9(6-7):684-94.
6. Alraies MC, and Eckman P. Adult heart transplant: indications and outcomes. *J Thorac Dis.* 2014;6(8):1120-8.
7. Herman DS, Lam L, Taylor MR, Wang L, Teekakirikul P, Christodoulou D, et al. Truncations of titin causing dilated cardiomyopathy. *N Engl J Med.* 2012;366(7):619-28.
8. Arbustini E, Pilotto A, Repetto A, Grasso M, Negri A, Diegoli M, et al. Autosomal dominant dilated cardiomyopathy with atrioventricular block: a lamin A/C defect-related disease. *J Am Coll Cardiol.* 2002;39(6):981-90.
9. Parks SB, Kushner JD, Nauman D, Burgess D, Ludwigsen S, Peterson A, et al. Lamin A/C mutation analysis in a cohort of 324 unrelated patients with idiopathic or familial dilated cardiomyopathy. *Am Heart J.* 2008;156(1):161-9.
10. Dobrzynska A, Gonzalo S, Shanahan C, and Askjaer P. The nuclear lamina in health and disease. *Nucleus.* 2016;7(3):233-48.
11. Fatkin D, MacRae C, Sasaki T, Wolff MR, Porcu M, Frenneaux M, et al. Missense mutations in the rod domain of the lamin A/C gene as causes of dilated cardiomyopathy and conduction-system disease. *N Engl J Med.* 1999;341(23):1715-24.
12. Taylor MR, Fain PR, Sinagra G, Robinson ML, Robertson AD, Carniel E, et al. Natural history of dilated cardiomyopathy due to lamin A/C gene mutations. *J Am Coll Cardiol.* 2003;41(5):771-80.
13. Schreiber KH, and Kennedy BK. When lamins go bad: nuclear structure and disease. *Cell.* 2013;152(6):1365-75.
14. Quarta G, Syrris P, Ashworth M, Jenkins S, Zuborne Alapi K, Morgan J, et al. Mutations in the Lamin A/C gene mimic arrhythmogenic right ventricular cardiomyopathy. *Eur Heart J.* 2012;33(9):1128-36.
15. Anselme F, Moubarak G, Savoure A, Godin B, Borz B, Drouin-Garraud V, et al. Implantable cardioverter-defibrillators in lamin A/C mutation carriers with cardiac conduction disorders. *Heart Rhythm.* 2013;10(10):1492-8.
16. Bonne G, Di Barletta MR, Varnous S, Becane HM, Hammouda EH, Merlini L, et al. Mutations in the gene encoding lamin A/C cause autosomal dominant Emery-Dreifuss muscular dystrophy. *Nat Genet.* 1999;21(3):285-8.
17. Brodsky GL, Muntoni F, Miocic S, Sinagra G, Sewry C, and Mestroni L. Lamin A/C gene mutation associated with dilated cardiomyopathy with variable skeletal muscle involvement. *Circulation.* 2000;101(5):473-6.
18. van Berlo JH, de Voogt WG, van der Kooi AJ, van Tintelen JP, Bonne G, Yaou RB, et al. Meta-analysis of clinical characteristics of 299 carriers of LMNA gene mutations: do lamin A/C mutations portend a high risk of sudden death? *J Mol Med (Berl).* 2005;83(1):79-83.
19. van Berlo JH, Duboc D, and Pinto YM. Often seen but rarely recognised: cardiac complications of lamin A/C mutations. *Eur Heart J.* 2004;25(10):812-4.

20. van Tintelen JP, Hofstra RM, Katerberg H, Rossenbacker T, Wiesfeld AC, du Marchie Sarvaas GJ, et al. High yield of LMNA mutations in patients with dilated cardiomyopathy and/or conduction disease referred to cardiogenetics outpatient clinics. *Am Heart J.* 2007;154(6):1130-9.
21. Chen SN, Lombardi R, Karmouch J, Tsai JY, Czernuszewicz G, Taylor MRG, et al. DNA Damage Response/TP53 Pathway Is Activated and Contributes to the Pathogenesis of Dilated Cardiomyopathy Associated With LMNA (Lamin A/C) Mutations. *Circ Res.* 2019;124(6):856-73.
22. Redwood AB, Perkins SM, Vanderwaal RP, Feng Z, Biehl KJ, Gonzalez-Suarez I, et al. A dual role for A-type lamins in DNA double-strand break repair. *Cell Cycle.* 2011;10(15):2549-60.
23. Graziano S, Kreienkamp R, Coll-Bonfill N, and Gonzalo S. Causes and consequences of genomic instability in laminopathies: Replication stress and interferon response. *Nucleus.* 2018;9(1):258-75.
24. Gibbs-Seymour I, Markiewicz E, Bekker-Jensen S, Mailand N, and Hutchison CJ. Lamin A/C-dependent interaction with 53BP1 promotes cellular responses to DNA damage. *Aging Cell.* 2015;14(2):162-9.
25. Cho S, Vashisth M, Abbas A, Majkut S, Vogel K, Xia Y, et al. Mechanosensing by the Lamina Protects against Nuclear Rupture, DNA Damage, and Cell-Cycle Arrest. *Dev Cell.* 2019;49(6):920-35 e5.
26. Stroud MJ, Banerjee I, Veevers J, and Chen J. Linker of nucleoskeleton and cytoskeleton complex proteins in cardiac structure, function, and disease. *Circ Res.* 2014;114(3):538-48.
27. Lee J, Termglinchan V, Diecke S, Itzhaki I, Lam CK, Garg P, et al. Activation of PDGF pathway links LMNA mutation to dilated cardiomyopathy. *Nature.* 2019.
28. Auguste G, Gurha P, Lombardi R, Coarfa C, Willerson JT, and Marian AJ. Suppression of Activated FOXO Transcription Factors in the Heart Prolongs Survival in a Mouse Model of Laminopathies. *Circ Res.* 2018.
29. Rober RA, Weber K, and Osborn M. Differential timing of nuclear lamin A/C expression in the various organs of the mouse embryo and the young animal: a developmental study. *Development.* 1989;105(2):365-78.
30. van Steensel B, and Belmont AS. Lamina-Associated Domains: Links with Chromosome Architecture, Heterochromatin, and Gene Repression. *Cell.* 2017;169(5):780-91.
31. Cheedipudi SM, Matkovich SJ, Coarfa C, Hu X, Robertson MJ, Sweet M, et al. Genomic Reorganization of Lamin-Associated Domains in Cardiac Myocytes Is Associated With Differential Gene Expression and DNA Methylation in Human Dilated Cardiomyopathy. *Circ Res.* 2019;124(8):1198-213.
32. Meuleman W, Peric-Hupkes D, Kind J, Beaudry JB, Pagie L, Kellis M, et al. Constitutive nuclear lamina-genome interactions are highly conserved and associated with A/T-rich sequence. *Genome Res.* 2013;23(2):270-80.
33. Peric-Hupkes D, Meuleman W, Pagie L, Bruggeman SW, Solovei I, Brugman W, et al. Molecular maps of the reorganization of genome-nuclear lamina interactions during differentiation. *Mol Cell.* 2010;38(4):603-13.
34. Kim Y, and Zheng Y. Generation and characterization of a conditional deletion allele for Lmna in mice. *Biochem Biophys Res Commun.* 2013;440(1):8-13.
35. Agah R, Frenkel PA, French BA, Michael LH, Overbeek PA, and Schneider MD. Gene recombination in postmitotic cells. Targeted expression of Cre recombinase provokes cardiac-restricted, site-specific rearrangement in adult ventricular muscle in vivo. *J Clin Invest.* 1997;100(1):169-79.
36. Bergmann O, Zdunek S, Alkass K, Druid H, Bernard S, and Frisen J. Identification of cardiomyocyte nuclei and assessment of ploidy for the analysis of cell turnover. *Exp Cell Res.* 2011;317(2):188-94.
37. Bergmann O, and Jovinge S. Isolation of cardiomyocyte nuclei from post-mortem tissue. *J Vis Exp.* 2012(65).
38. Preissl S, Schwaderer M, Raulf A, Hesse M, Gruning BA, Kobele C, et al. Deciphering the Epigenetic Code of Cardiac Myocyte Transcription. *Circ Res.* 2015;117(5):413-23.

39. Anand P, Brown JD, Lin CY, Qi J, Zhang R, Artero PC, et al. BET bromodomains mediate transcriptional pause release in heart failure. *Cell.* 2013;154(3):569-82.
40. Stratton MS, Haldar SM, and McKinsey TA. BRD4 inhibition for the treatment of pathological organ fibrosis. *F1000Res.* 2017;6.
41. Duan Q, McMahon S, Anand P, Shah H, Thomas S, Salunga HT, et al. BET bromodomain inhibition suppresses innate inflammatory and profibrotic transcriptional networks in heart failure. *Sci Transl Med.* 2017;9(390).
42. Stratton MS, Bagchi RA, Felisbino MB, Hirsch RA, Smith HE, Riching AS, et al. Dynamic Chromatin Targeting of BRD4 Stimulates Cardiac Fibroblast Activation. *Circ Res.* 2019;125(7):662-77.
43. Song S, Liu L, Yu Y, Zhang R, Li Y, Cao W, et al. Inhibition of BRD4 attenuates transverse aortic constriction- and TGF-beta-induced endothelial-mesenchymal transition and cardiac fibrosis. *J Mol Cell Cardiol.* 2019;127:83-96.
44. Filippakopoulos P, Qi J, Picaud S, Shen Y, Smith WB, Fedorov O, et al. Selective inhibition of BET bromodomains. *Nature.* 2010;468(7327):1067-73.
45. Senyo SE, Lee RT, and Kuhn B. Cardiac regeneration based on mechanisms of cardiomyocyte proliferation and differentiation. *Stem Cell Res.* 2014;13(3 Pt B):532-41.
46. Mahmoud AI, Kocabas F, Muralidhar SA, Kimura W, Koura AS, Thet S, et al. Meis1 regulates postnatal cardiomyocyte cell cycle arrest. *Nature.* 2013;497(7448):249-53.
47. Porrello ER, Mahmoud AI, Simpson E, Hill JA, Richardson JA, Olson EN, et al. Transient regenerative potential of the neonatal mouse heart. *Science.* 2011;331(6020):1078-80.
48. Segatto M, Fittipaldi R, Pin F, Sartori R, Dae Ko K, Zare H, et al. Epigenetic targeting of bromodomain protein BRD4 counteracts cancer cachexia and prolongs survival. *Nat Commun.* 2017;8(1):1707.
49. Winter GE, Mayer A, Buckley DL, Erb MA, Roderick JE, Vittori S, et al. BET Bromodomain Proteins Function as Master Transcription Elongation Factors Independent of CDK9 Recruitment. *Mol Cell.* 2017;67(1):5-18 e9.
50. Newman MS, Nguyen T, Watson MJ, Hull RW, and Yu HG. Transcriptome profiling reveals novel BMI- and sex-specific gene expression signatures for human cardiac hypertrophy. *Physiol Genomics.* 2017;49(7):355-67.
51. Tsybouleva N, Zhang L, Chen S, Patel R, Lutucuta S, Nemoto S, et al. Aldosterone, through novel signaling proteins, is a fundamental molecular bridge between the genetic defect and the cardiac phenotype of hypertrophic cardiomyopathy. *Circulation.* 2004;109(10):1284-91.
52. Lutucuta S, Tsybouleva N, Ishiyama M, Defreitas G, Wei L, Carabello B, et al. Induction and reversal of cardiac phenotype of human hypertrophic cardiomyopathy mutation cardiac troponin T-Q92 in switch on-switch off bigenic mice. *J Am Coll Cardiol.* 2004;44(11):2221-30.
53. Arimura T, Helbling-Leclerc A, Massart C, Varnous S, Niel F, Lacene E, et al. Mouse model carrying H222P-Lmna mutation develops muscular dystrophy and dilated cardiomyopathy similar to human striated muscle laminopathies. *Hum Mol Genet.* 2005;14(1):155-69.
54. Mounkes LC, Kozlov SV, Rottman JN, and Stewart CL. Expression of an LMNA-N195K variant of A-type lamins results in cardiac conduction defects and death in mice. *Hum Mol Genet.* 2005;14(15):2167-80.
55. Wu SY, and Chiang CM. The double bromodomain-containing chromatin adaptor Brd4 and transcriptional regulation. *J Biol Chem.* 2007;282(18):13141-5.
56. Wang R, Cao XJ, Kulej K, Liu W, Ma T, MacDonald M, et al. Uncovering BRD4 hyperphosphorylation associated with cellular transformation in NUT midline carcinoma. *Proc Natl Acad Sci U S A.* 2017;114(27):E5352-E61.
57. Huang H, Tang Q, Chu H, Jiang J, Zhang H, Hao W, et al. MAP4K4 deletion inhibits proliferation and activation of CD4(+) T cell and promotes T regulatory cell generation in vitro. *Cell Immunol.* 2014;289(1-2):15-20.

58. Zohn IE, Li Y, Skolnik EY, Anderson KV, Han J, and Niswander L. p38 and a p38-interacting protein are critical for downregulation of E-cadherin during mouse gastrulation. *Cell.* 2006;125(5):957-69.
59. Cheedipudi SM, Hu J, Fan S, Yuan P, Karmouch J, Czernuszewicz G, et al. Exercise Restores Dysregulated Gene Expression in a Mouse Model of Arrhythmogenic Cardiomyopathy. *Cardiovasc Res.* 2019.
60. Karmouch J, Zhou QQ, Miyake CY, Lombardi R, Kretzschmar K, Bannier-Helaouet M, et al. Distinct Cellular Basis for Early Cardiac Arrhythmias, the Cardinal Manifestation of Arrhythmogenic Cardiomyopathy, and the Skin Phenotype of Cardiocutaneous Syndromes. *Circ Res.* 2017;121(12):1346-59.
61. Law CW, Chen Y, Shi W, and Smyth GK. voom: Precision weights unlock linear model analysis tools for RNA-seq read counts. *Genome Biol.* 2014;15(2):R29.
62. Frankish A, Diekhans M, Ferreira AM, Johnson R, Jungreis I, Loveland J, et al. GENCODE reference annotation for the human and mouse genomes. *Nucleic Acids Res.* 2019;47(D1):D766-D73.
63. Love MI, Huber W, and Anders S. Moderated estimation of fold change and dispersion for RNA-seq data with DESeq2. *Genome Biol.* 2014;15(12):550.
64. Risso D, Ngai J, Speed TP, and Dudoit S. Normalization of RNA-seq data using factor analysis of control genes or samples. *Nat Biotechnol.* 2014;32(9):896-902.
65. Subramanian A, Tamayo P, Mootha VK, Mukherjee S, Ebert BL, Gillette MA, et al. Gene set enrichment analysis: a knowledge-based approach for interpreting genome-wide expression profiles. *Proc Natl Acad Sci U S A.* 2005;102(43):15545-50.
66. Zhang Y, Liu T, Meyer CA, Eeckhoute J, Johnson DS, Bernstein BE, et al. Model-based analysis of ChIP-Seq (MACS). *Genome Biol.* 2008;9(9):R137.
67. Lerdrup M, Johansen JV, Agrawal-Singh S, and Hansen K. An interactive environment for agile analysis and visualization of ChIP-sequencing data. *Nat Struct Mol Biol.* 2016;23(4):349-57.
68. Robinson JT, Thorvaldsdottir H, Winckler W, Guttman M, Lander ES, Getz G, et al. Integrative genomics viewer. *Nat Biotechnol.* 2011;29(1):24-6.

FIGURE LEGENDS

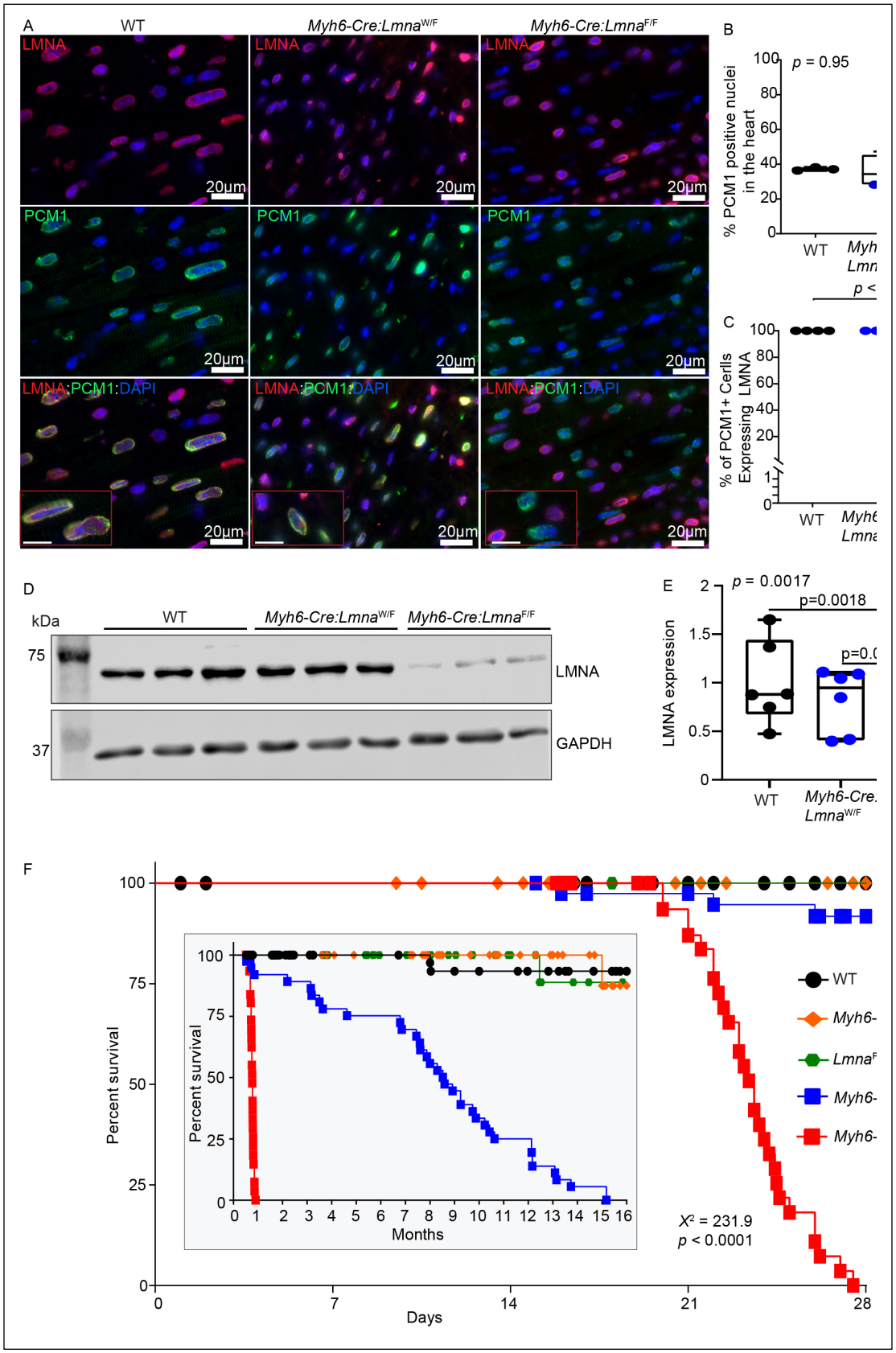

Figure 1: Conditional deletion of *Lmna* gene in cardiac myocyte in mice. A. Representative immunofluorescence staining of thin myocardial section from 3 weeks old WT, *Myh6-Cre*:*Lmna*$^{W/F}$ and *Myh6-Cre*:*Lmna*$^{F/F}$ mice showing localization of LMNA (red) at the nuclear membrane in PCM1-labeled (green) cardiac myocytes. Nuclei were counterstained with DAPI (blue). Scale bar is 20 μm and 10 μm in the inserts. **B.** Quantitative data of PCM1-labeled nuclei in WT (N=3), *Myh6-Cre*:*Lmna*$^{W/F}$ (N=4) and *Myh6-Cre*:*Lmna*$^{F/F}$ (N=5, $p = 0.95$). **C.** Quantitative data of PCM1-labeled nuclei showing expression of LMNA in WT, *Myh6-Cre*:*Lmna*$^{W/F}$ and *Myh6-Cre*:*Lmna*$^{F/F}$ (N=5, $p < 0.0001$). **D.** Western blots showing expression of LMNA in isolated cardiac myocyte cell lysates in 2 weeks old WT, *Myh6-Cre*:*Lmna*$^{W/F}$ and *Myh6-Cre*:*Lmna*$^{F/F}$ and the corresponding GAPDH, as a loading control. **E.** Quantitative data on LMNA expression levels in cardiac myocyte in the WT (N=6), *Myh6-Cre*:*Lmna*$^{W/F}$ (N=6) and *Myh6-Cre*:*Lmna*$^{F/F}$ (N=6 mice; $p = 0.0017$). **F.** Kaplan-Meier curve showing the survival of WT (N=52), *Myh6-Cre* (N=38), *Lmna*$^{F/F}$ (N= 50), *Myh6-Cre*:*Lmna*$^{W/F}$ (N=40) and *Myh6-Cre*:*Lmna*$^{F/F}$ (N=37) mice during the first 4 weeks (X^2=231, p<0.0001) and 16 months (inset; X^2=344, p<0.0001) after birth. P values shown in C, D an E panels were calculated by ordinary One-way ANOVA, and Tukey *post-hoc* pairwise comparison test, were * $p < 0.05$ and ** $p < 0.01$.

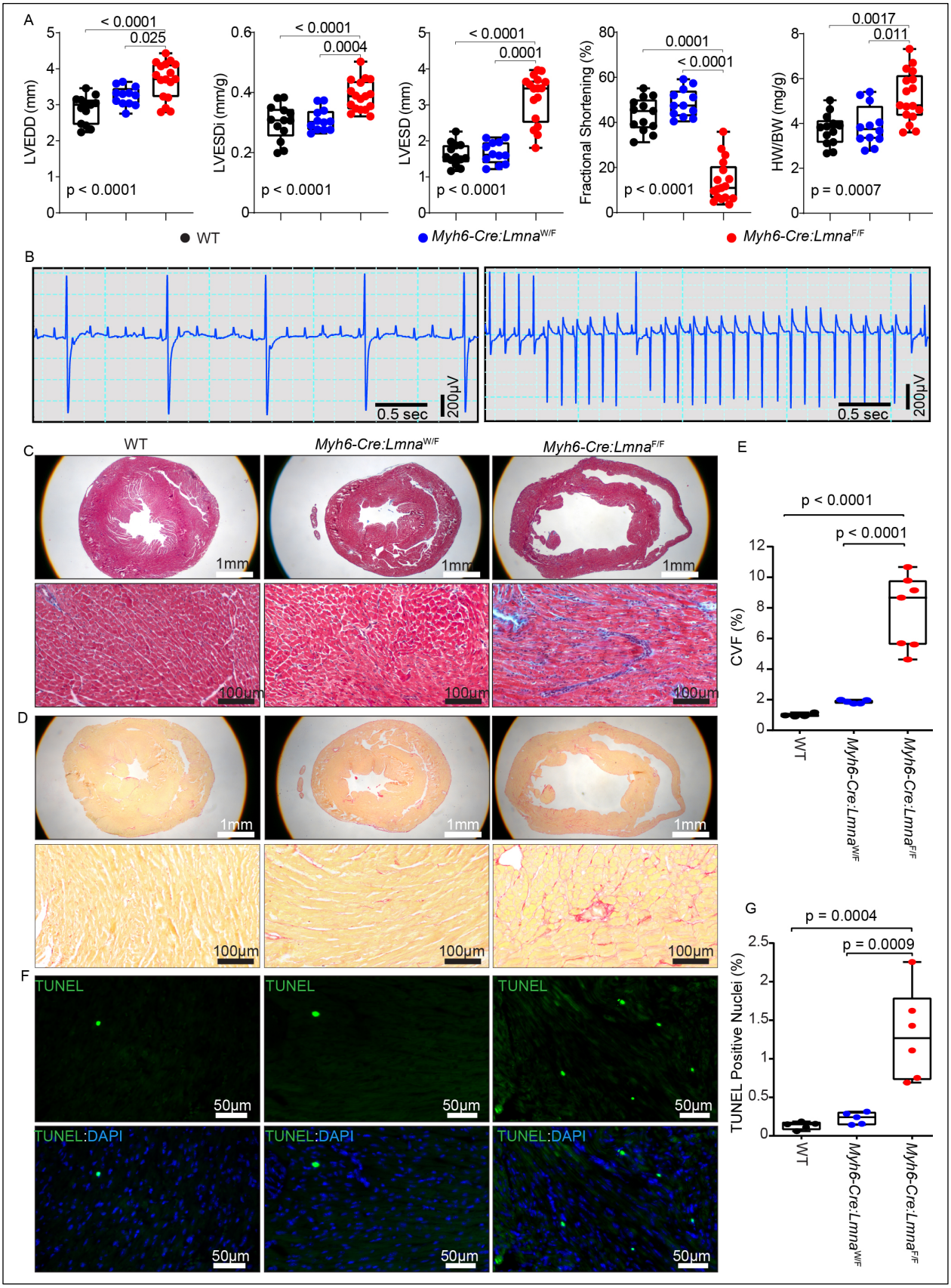
A
LVEDD (mm)
< 0.0001
0.025
p < 0.0001
LVESDi (mm/g)
< 0.0001
0.0004
p < 0.0001
LVESD (mm)
< 0.0001
0.0001
p < 0.0001
Fractional Shortening (%)
0.0001
< 0.0001
p < 0.0001
HW/BW (mg/g)
0.0017
0.011
p = 0.0007
WT
Myh6-Cre:Lmna W/F
Myh6-Cre:Lmna F/F
B
0.5 sec
200µV
0.5 sec
200µV
C
WT
Myh6-Cre:Lmna W/F
Myh6-Cre:Lmna F/F
1mm
100µm
D
1mm
100µm
E
p < 0.0001
p < 0.0001
CVF (%)
WT
Myh6-Cre:Lmna W/F
Myh6-Cre:Lmna F/F
F
TUNEL
TUNEL:DAPI
50µm
G
p = 0.0004
p = 0.0009
TUNEL Positive Nuclei (%)
WT
Myh6-Cre:Lmna W/F
Myh6-Cre:Lmna F/F

Figure 2: Cardiac phenotype in 3 weeks old WT, *Myh6-Cre*:*Lmna*$^{W/F}$, and *Myh6-Cre*:*Lmna*$^{F/F}$ mice. **A**. Selected echocardiographic parameters showing left ventricular end-diastolic diameter (LVEDD), left ventricular end-systolic diameter (LVESD), left ventricular end-systolic diameter indexed to body weight (LVESD), left ventricular fractional shortening (LVFS), and the left ventricular mass indexed to body weight (LVMI) in 3 weeks old WT (N=13), *Myh6-Cre*:*Lmna*$^{W/F}$ (N=12) and *Myh6-Cre*:*Lmna*$^{F/F}$ (N=17) mice. P value shown were obtained using Ordinary One-way ANOVA and Bonferroni *post hoc* test for comparisons of the LVEDD, LVESDi and LVMI, and Kruskal-Wallis and Dunn's *post hoc* test for comparisons for LVESD and LVFS. **B.** Selected representative surface ECG recordings showing third-degree AV-block (no association between P and QRS waves) and ventricular tachycardia (VT) observed in the *Myh6-Cre*:*Lmna*$^{W/F}$ (N=19) and *Myh6-Cre*:*Lmna*$^{F/F}$ mice (N=19)**C** and **D.** Masson's Trichrome (upper panel) and Picrosirius red (lower panel) stained representative myocardial sections in 3 weeks old WT, *Myh6-Cre*:*Lmna*$^{W/F}$, and *Myh6-Cre*:*Lmna*$^{F/F}$ mice. **E.** Corresponding quantitative data on percent collagen volume fraction (CVF) in myocardial sections in the WT (N=4), *Myh6-Cre*:*Lmna*$^{W/F}$ (N=5), and *Myh6-Cre*:*Lmna*$^{F/F}$ (N=7) mice. **F.** TUNEL stained thin myocardial sections in 3 weeks old WT, *Myh6-Cre*:*Lmna*$^{W/F}$, and *Myh6-Cre*:*Lmna*$^{F/F}$ mice. TUNEL positive cells are shown in green and nuclei, counterstained with DAPI, in blue. **G.** Quantitative data showing percentage of TUNEL positive nuclei in the WT (N=5), *Myh6-Cre*:*Lmna*$^{W/F}$ (N=5), and *Myh6-Cre*:*Lmna*$^{F/F}$ (N=6) mice. P values shown in panel E and G were calculated using Ordinary One-way ANOVA and Tukey post hoc test.

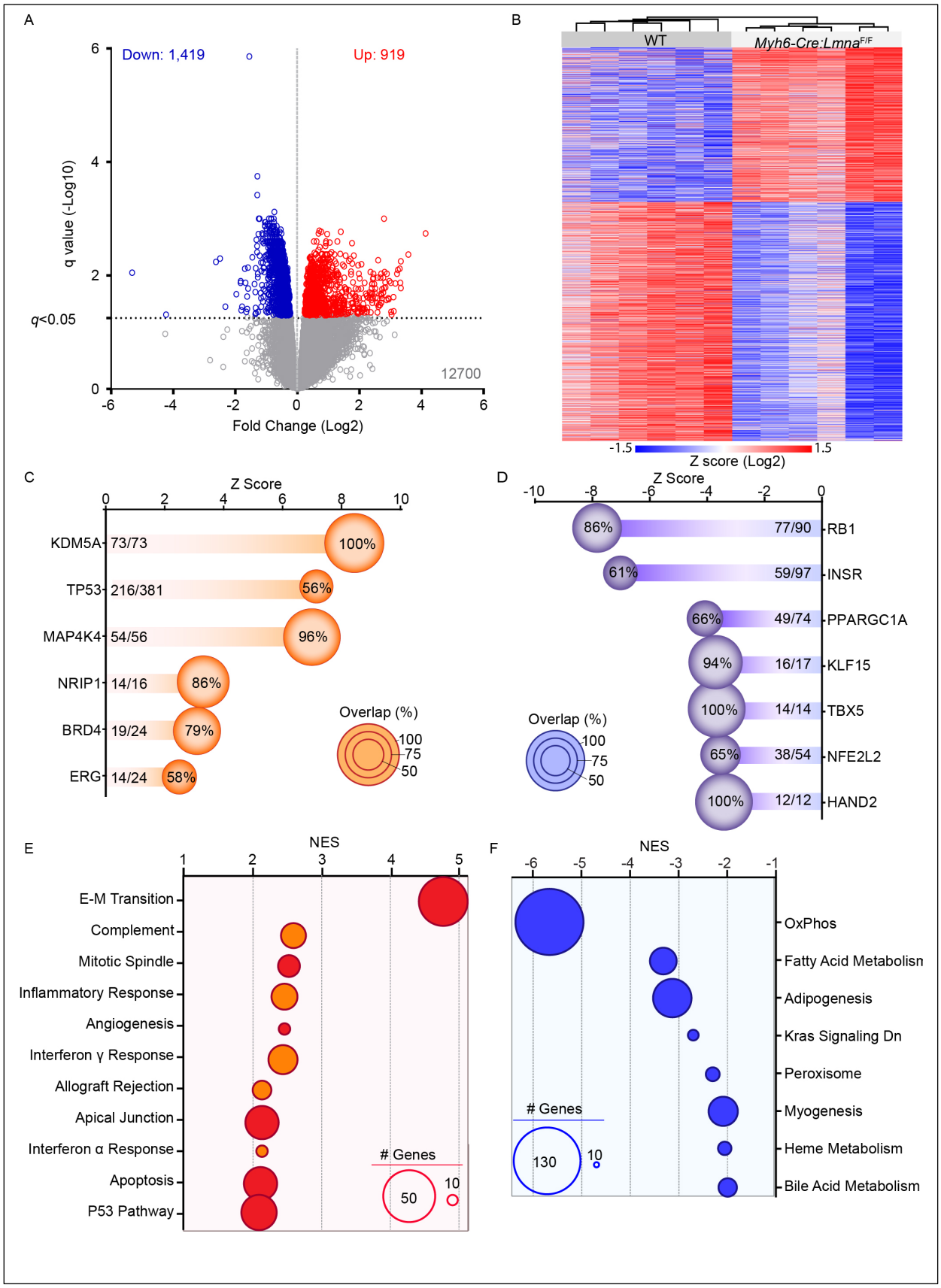
A
Down: 1,419
Up: 919
q value (-Log10)
q<0.05
12700
Fold Change (Log2)
B
WT
Myh6-Cre:Lmna F/F
-1.5
1.5
Z score (Log2)
C
Z Score
KDM5A 73/73 100%
TP53 216/381 56%
MAP4K4 54/56 96%
NRIP1 14/16 86%
BRD4 19/24 79%
ERG 14/24 58%
Overlap (%)
100
75
50
D
Z Score
86% 77/90 RB1
61% 59/97 INSR
66% 49/74 PPARGC1A
94% 16/17 KLF15
100% 14/14 TBX5
65% 38/54 NFE2L2
100% 12/12 HAND2
Overlap (%)
100
75
50
E
NES
E-M Transition
Complement
Mitotic Spindle
Inflammatory Response
Angiogenesis
Interferon γ Response
Allograft Rejection
Apical Junction
Interferon α Response
Apoptosis
P53 Pathway
Genes
50
10
F
NES
OxPhos
Fatty Acid Metabolism
Adipogenesis
Kras Signaling Dn
Peroxisome
Myogenesis
Heme Metabolism
Bile Acid Metabolism
Genes
130
10

Figure 3: Differentially expressed genes (DEGs) in 2 weeks old WT and *Myh6-Cre*:*Lmna*$^{F/F}$ mouse cardiac myocytes. A. Volcano Plot depicting DEGs showing down-regulation of 1,419 and upregulation of 919 genes in the *Myh6-Cre*:*Lmna*$^{F/F}$ (N=6) compared to WT mouse cardiac myocytes (N=6). **B.** Heat Map and unsupervised hierarchical clustering of the DEGs in the WT and the *Myh6-Cre*:*Lmna*$^{F/F}$ mouse cardiac myocytes, showing clustering according to the genotype. **C** and **D**. Ingenuity Pathway Analysis (IPA) for inferred activated (**C**) and suppressed (**D**) upstream regulators of the DEGs in the *Myh6-Cre*:*Lmna*$^{F/F}$ mouse cardiac myocytes. Z-score and percentage of overlap of the DEGs with the IPA database are depicted on the graphs. Size of each circle is proportional to percent of genes considered as downstream target of each regulator in the RNA-Seq dataset. **E** and **F**. Top significantly enriched Hallmark pathways activated (**E**) or inhibited (**F**) inferred using Gene Set Enrichment Analysis (GSEA). Normalized enrichment score (NES) and number of genes involved (size of the circle) are depicted for each pathway.

Figure 4: Evidence of BET bromodomain activation in the *Myh6-Cre*:*Lmna*$^{F/F}$ mouse cardiac myocytes. A. GSEA plot of DEGs in the *Myh6-Cre*:*Lmna*$^{F/F}$ mouse cardiac myocytes against predicted BRDs target genes gathered, from whole mouse heart after transaortic constriction or myocardial infarction, respectively (GSE96561, GSE96561, and GSE48110), and in rat neonatal ventricular cardiac myocytes (NVRM; GSE83228). **B.** GSEA of DEGs in the *Myh6-Cre*:*Lmna*$^{F/F}$ mouse cardiac myocytes against predicted BRDs target genes obtained from IPA **C.** Heat map and unsupervised hierarchical clustering of 145 DEGs in the *Myh6-Cre*:*Lmna*$^{F/F}$ mouse cardiac myocytes obtained after overlapping with the GSEA data shown in **A** and **B**.

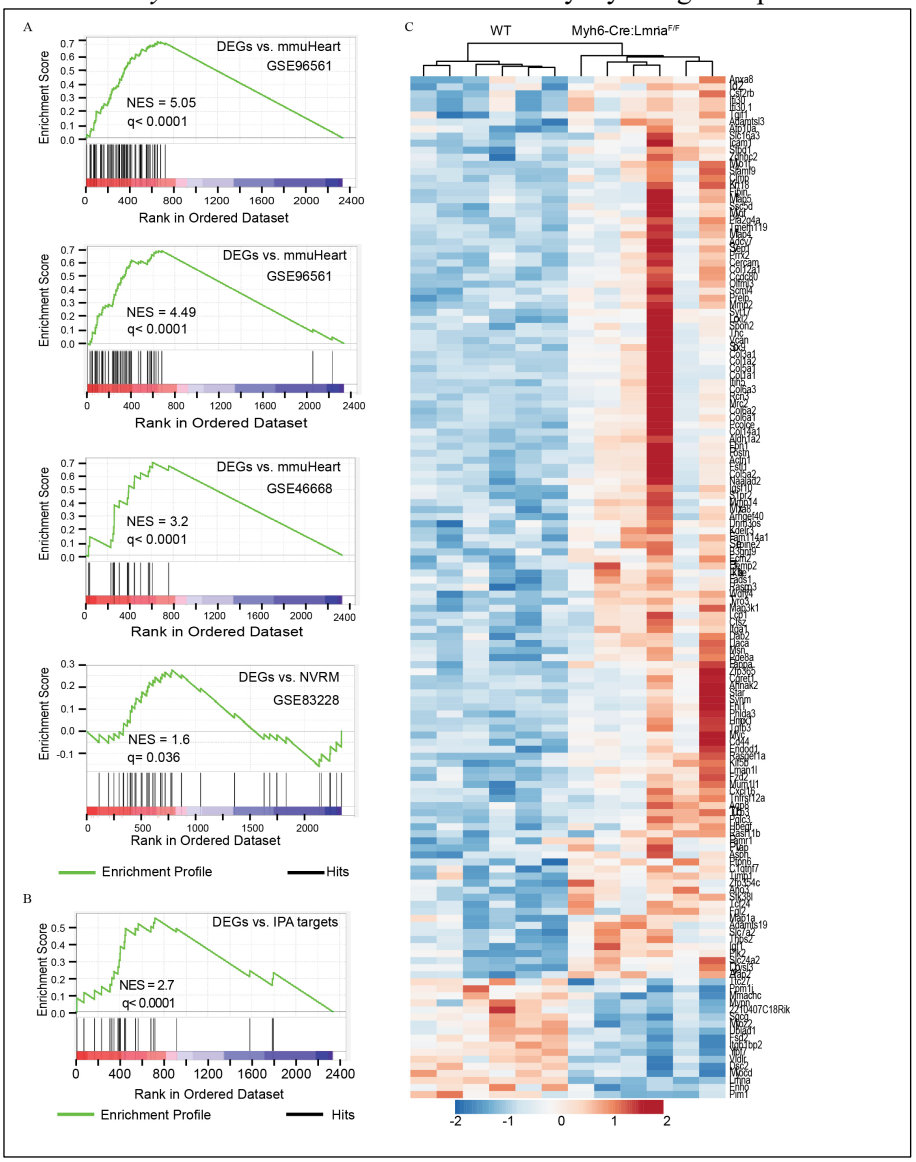

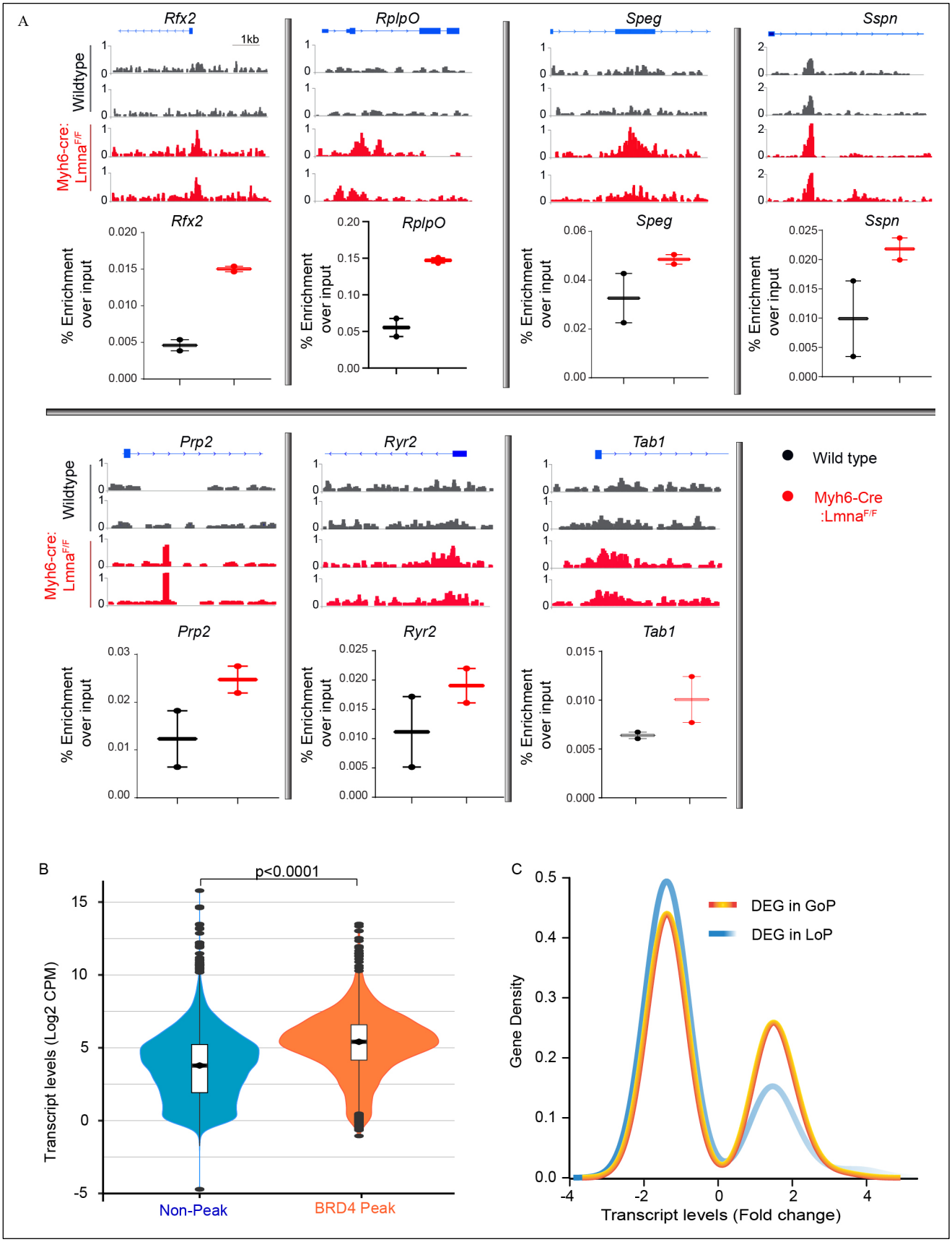

Figure 5: BRD4 activation in the *Myh6-Cre*:*Lmna*$^{F/F}$ mouse cardiac myocytes. A. ChIP-qPCR in the

WT and *Myh6-Cre*:*Lmna*$^{F/F}$ mouse cardiac myocytes chromatin extracts (N=2 for each genotype) and IGV tracks from the ChIP-seq showing BRD4 enrichment in the corresponding regions assessed. **B.** Violin plots depicting transcript levels of all genes at non-peak and BRD4 peak regions in the *Myh6-Cre*:*Lmna*$^{F/F}$ mouse cardiac myocytes (p<0.0001 by Kruskal-Wallis). **C.** Transcript levels of DEGs plotted against gene density at the GoP and LoP genomic regions, showing a higher density of genes with increased transcript levels in the GoP regions.

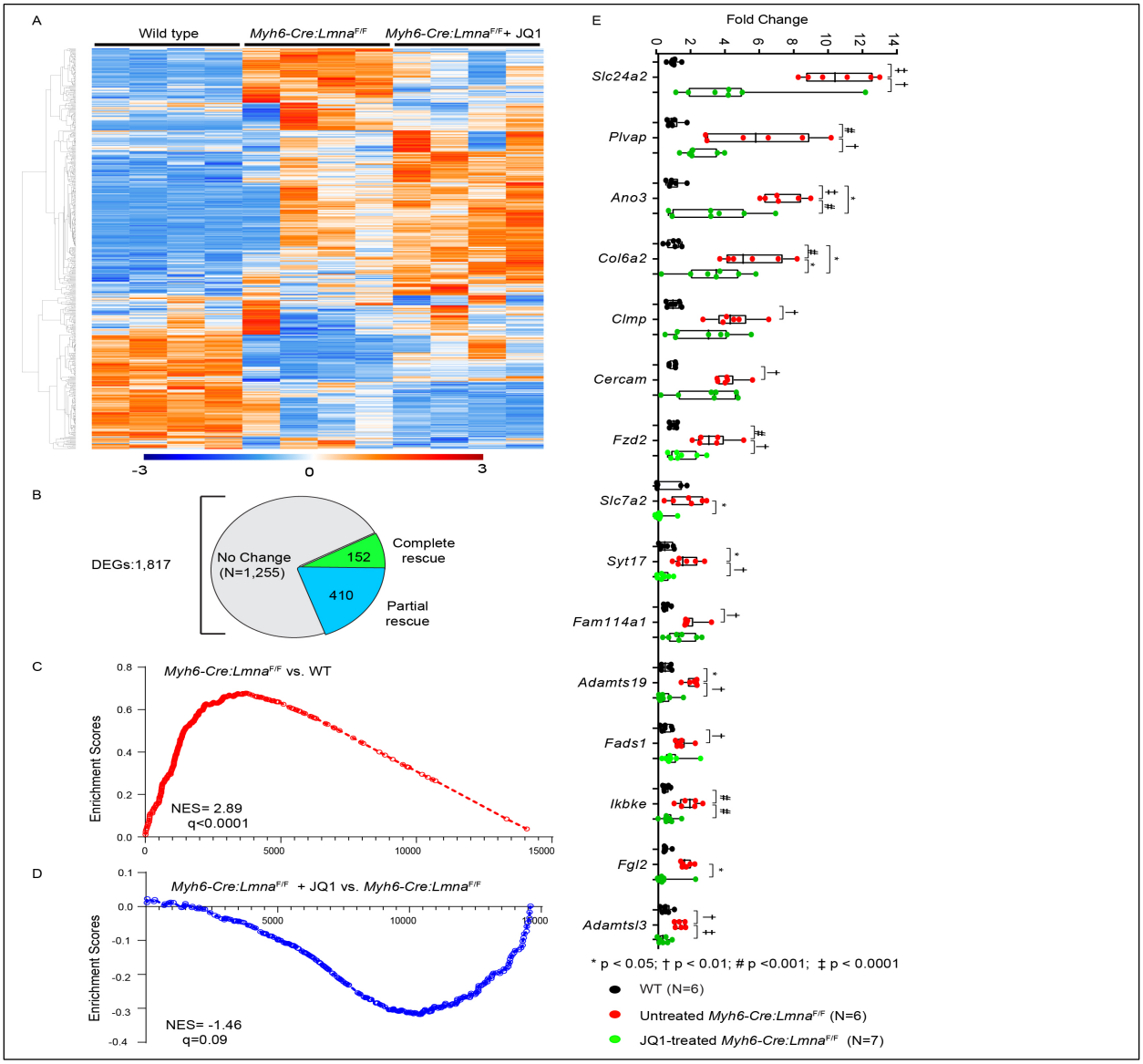

Figure 6: Effect of BET bromodomain inhibition on the transcriptome of *Myh6-Cre*:*Lmna*$^{F/F}$ mouse cardiac myocytes:A. Heat Map of the DEGs in the WT, the *Myh6-Cre*:*Lmna*$^{F/F}$ and the JQ1-treated *Myh6-Cre*:*Lmna*$^{F/F}$ mouse cardiac myocytes (N=4 for each). **B.** Pie chart depicting the number of genes that were rescued and partially rescued upon JQ1-treatment in the *Myh6-Cre*:*Lmna*$^{F/F}$ mouse cardiac myocytes from the differentially expressed genes between the WT and *Myh6-Cre:Lmna*$^{F/F}$ myocytes. **C.** GSEA plots of the BRD4 target genes showing induction in the *Myh6-Cre*:*Lmna*$^{F/F}$ compared to the WT cardiac myocytes (NES=2.89, q<0.0001), and partially suppressed in the JQ1-treated *Myh6-Cre*:*Lmna*$^{F/F}$ compared to the *Myh6-Cre*:*Lmna*$^{F/F}$ (NES=-1.46, q=0.09). **D.** RT-qPCR data showing transcript levels of selected BRD4

target genes in the WT (N=6), untreated (N=6) and JQ1-treated *Myh6-Cre*:*Lmna*$^{F/F}$ mouse cardiac myocytes (N=7), p values were obtained with Ordinary One-way ANOVA or Kruskal-Wallis where * $p < 0.05$; † $p < 0.01$; # $p < 0.001$; ‡ $p < 0.0001$.

Figure 7: Upstream regulators and biological pathways altered after BET bromodomain inhibition in *Myh6-Cre*:*Lmna*$^{F/F}$ mouse cardiac myocytes: A. Major putative inferred upstream regulators and their targets from IPA overlap analysis of the completely and partially rescued genes upon JQ1-treatment in the *Myh6-Cre*:*Lmna*$^{F/F}$. **B.** Circos Plot showing the top significantly enriched Hallmark pathways inferred from the completely and partially rescued genes upon JQ1-treatment in the *Myh6-Cre*:*Lmna*$^{F/F}$ using GSEA, with the log2 fold change depicting the relative expression of the genes involved in these pathways, as followed I: *Myh6-Cre*:*Lmna*$^{F/F}$ compared to the WT cardiac myocytes; II: JQ1-treated *Myh6-Cre*:*Lmna*$^{F/F}$ compared to the *Myh6-Cre*:*Lmna*$^{F/F}$. **C.** GSEA plots of the EMT showing induction in the *Myh6-Cre*:*Lmna*$^{F/F}$ compared to the WT cardiac myocytes (NES=2.3, q<0.0001), and its partial suppression in the JQ1-treated *Myh6-Cre*:*Lmna*$^{F/F}$ compared to the *Myh6-Cre*:*Lmna*$^{F/F}$ (NES=-1.14, q=0.43).

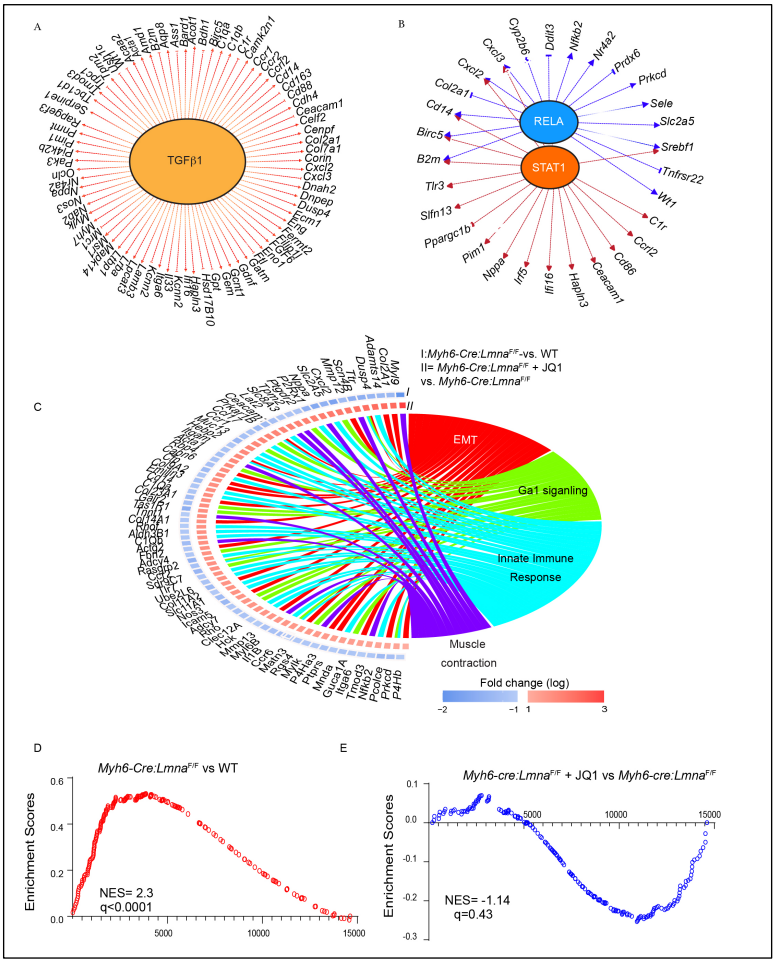

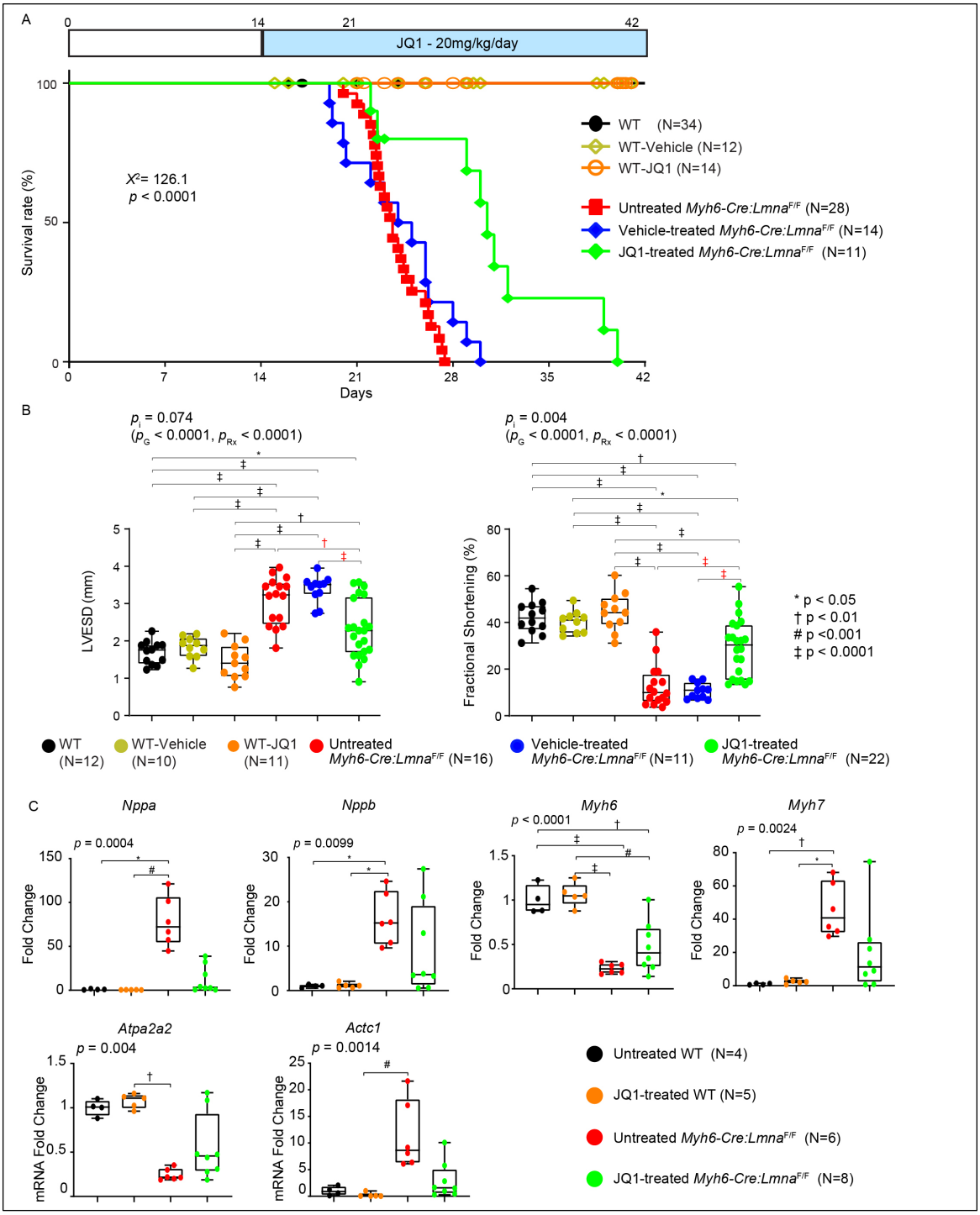

Figure 8: Phenotypic Effects of BET bromodomain proteins inhibition in *Myh6-Cre*:*Lmna*$^{F/F}$ mice. A. Kaplan-Meier survival curves in the untreated (black line; N=34), vehicle-treated (yellow line; N=12) and JQ1-treated WT (orange line; N=14), as well as untreated (red line; N=28), vehicle-treated (blue line; N=14) and JQ1-treated *Myh6-Cre*:*Lmna*$^{F/F}$ mice (green line, N=11) mice. **B.** Selected echocardiographic

parameters after one week of treatment in 3-week old untreated (black dots; N=12), vehicle-treated (yellow dots; N=10) and JQ1-treated WT (orange dots; N=11), as well as untreated (red dots; N=16), vehicle-treated (blue dots; N=11) and JQ1-treated (green dots, N=22) *Myh6-Cre*:*Lmna*$^{F/F}$ mice. P values shown were obtained using 2 Way ANOVA and Bonferroni *post hoc* test for comparisons where * $p < 0.05$; † $p < 0.01$; # $p < 0.001$; ‡ $p < 0.0001$. **C.** Expression levels of known markers of cardiac dysfunction, quantified by RT-qPCR, after one week of treatment in 3-week old untreated (black dots; N=4), and JQ1-treated WT (orange dots; N=5) mice, as well as untreated (red dots; N=6), and JQ1-treated (green dots; N=8) *Myh6-Cre*:*Lmna*$^{F/F}$ mice. Because untreated and vehicle-treated mice were indistinguishable from each other, only untreated and JQ1 treated mice were analyzed. P values shown were obtained with Ordinary One-way ANOVA or Kruskal-Wallis where * $p < 0.05$; † $p < 0.01$; # $p < 0.001$; ‡ $p < 0.0001$

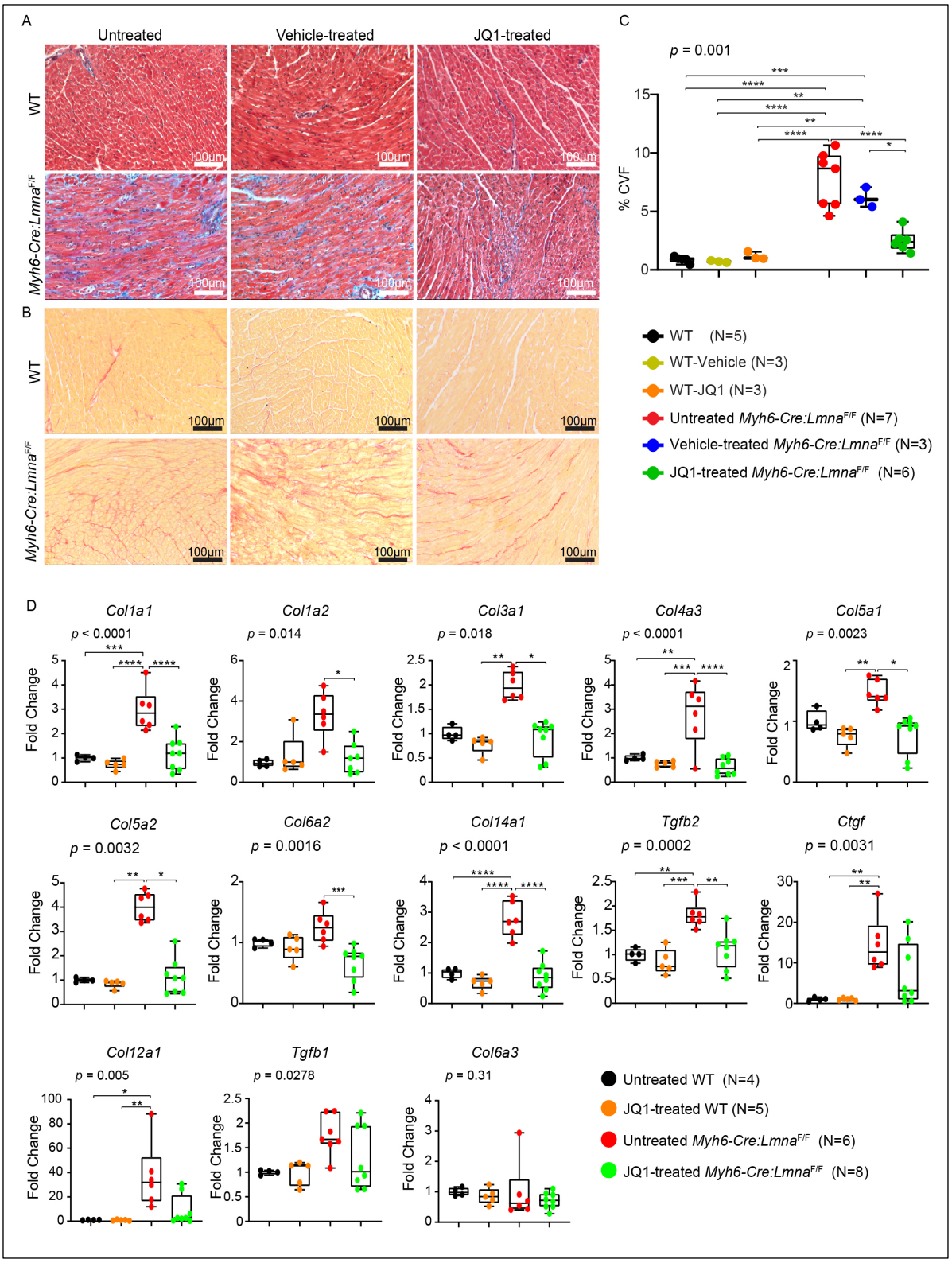
A
Untreated
Vehicle-treated
JQ1-treated
WT
Myh6-Cre:Lmna^F/F
100μm
B
C
p = 0.001
% CVF
WT (N=5)
WT-Vehicle (N=3)
WT-JQ1 (N=3)
Untreated Myh6-Cre:Lmna^F/F (N=7)
Vehicle-treated Myh6-Cre:Lmna^F/F (N=3)
JQ1-treated Myh6-Cre:Lmna^F/F (N=6)
D
Col1a1
p < 0.0001
Col1a2
p = 0.014
Col3a1
p = 0.018
Col4a3
p < 0.0001
Col5a1
p = 0.0023
Col5a2
p = 0.0032
Col6a2
p = 0.0016
Col14a1
p < 0.0001
Tgfb2
p = 0.0002
Ctgf
p = 0.0031
Col12a1
p = 0.005
Tgfb1
p = 0.0278
Col6a3
p = 0.31
Fold Change
Untreated WT (N=4)
JQ1-treated WT (N=5)
Untreated Myh6-Cre:Lmna^F/F (N=6)
JQ1-treated Myh6-Cre:Lmna^F/F (N=8)

Figure 9: Effect of BET bromodomain proteins inhibition on myocardial fibrosis in the *Myh6-Cre*:*Lmna*$^{F/F}$ mice. A and **B**. Representative Masson's Trichrome (upper panels) and Pico Sirius red (lower panels) stained myocardial sections after one week of treatment in 3-week old untreated, vehicle, and JQ1-treated WT and *Myh6-Cre*:*Lmna*$^{F/F}$ mice. **C.** Corresponding quantitative data showing the percent of CVF in the myocardial sections in untreated (black dots; N=5), vehicle-treated (yellow dots; N=3) and JQ1-treated WT (orange dots; N=3), as well as untreated (red dots; N=7), vehicle-treated (blue dots; N=3) and JQ1-treated (green dots; N=6) *Myh6-Cre*:*Lmna*$^{F/F}$ mice. P values were calculated using 2-way ANOVA and Tukey *post hoc* test for comparisons where *: $p < 0.05$, **: $p < 0.01$, ***: $p < 0.001$, ****: $p < 0.0001$. **D.** Transcript levels of selected BRD4 target genes involved in fibrosis in the heart as quantified by RT-qPCR in untreated (black dots; N=4), and JQ1-treated (orange dots; N=5) WT mice, as well as untreated (red dots; N=6), and JQ1-treated (green; N=8) *Myh6-Cre*:*Lmna*$^{F/F}$ mice. P values shown were obtained with Ordinary One-way ANOVA or Kruskal-Wallis where *: $p < 0.05$, **: $p < 0.01$, ***: $p < 0.001$, ****: $p < 0.0001$.

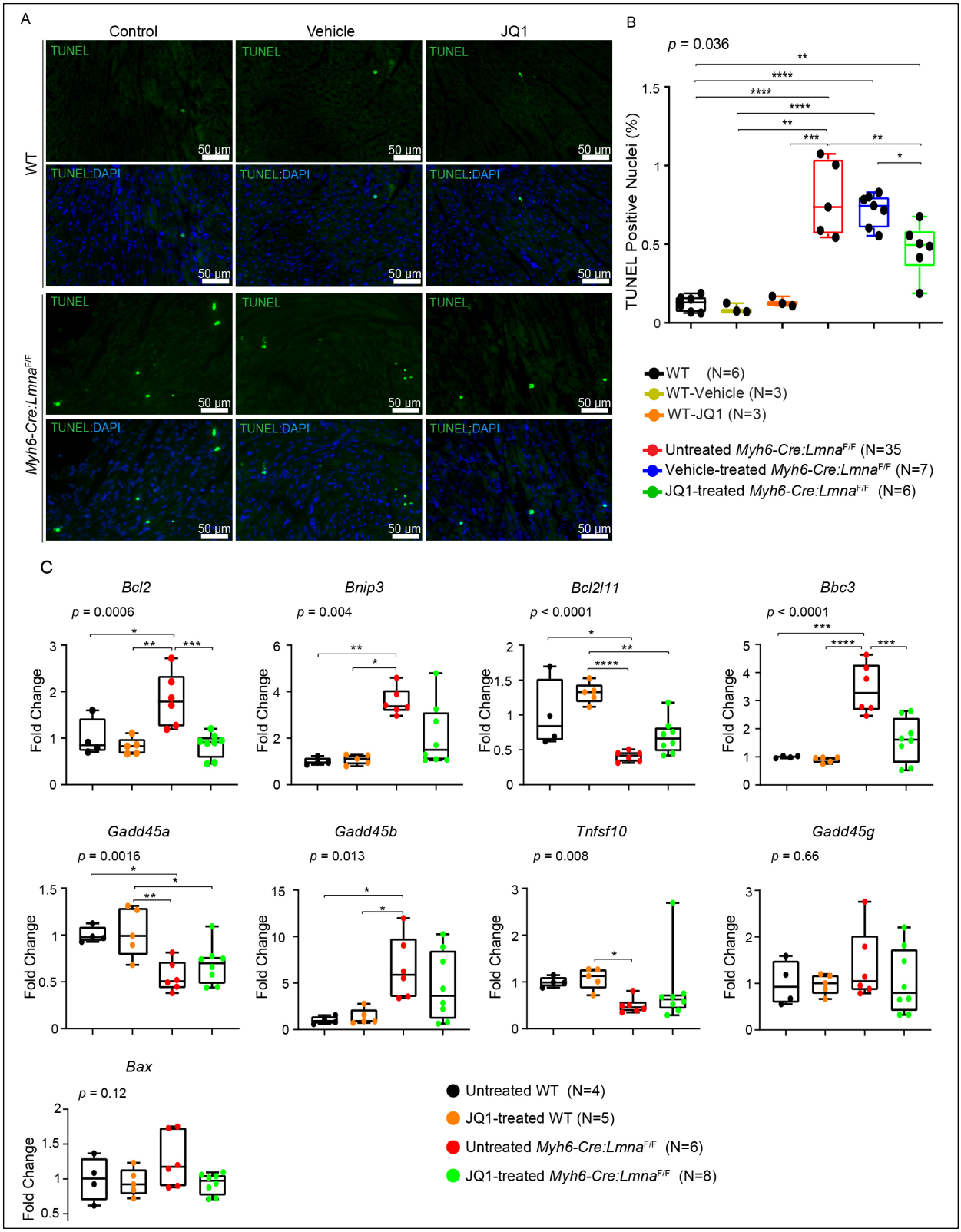
A
Control
Vehicle
JQ1
WT
Myh6-Cre:Lmna F/F
TUNEL
TUNEL:DAPI
50 µm
B
p = 0.036
TUNEL Positive Nuclei (%)
WT (N=6)
WT-Vehicle (N=3)
WT-JQ1 (N=3)
Untreated Myh6-Cre:Lmna F/F (N=35
Vehicle-treated Myh6-Cre:Lmna F/F (N=7)
JQ1-treated Myh6-Cre:Lmna F/F (N=6)
C
Bcl2
p = 0.0006
Bnip3
p = 0.004
Bcl2l11
p < 0.0001
Bbc3
p < 0.0001
Gadd45a
p = 0.0016
Gadd45b
p = 0.013
Tnfsf10
p = 0.008
Gadd45g
p = 0.66
Bax
p = 0.12
Fold Change
Untreated WT (N=4)
JQ1-treated WT (N=5)
Untreated Myh6-Cre:Lmna F/F (N=6)
JQ1-treated Myh6-Cre:Lmna F/F (N=8)

Figure 10: Effect of BET bromodomain proteins inhibition on myocardial apoptosis in the *Myh6-Cre*:*Lmna*$^{F/F}$ mice. A. Representative TUNEL stained thin myocardial sections in 3-weeks old untreated, vehicle-treated, and JQ1-treated WT mice along with untreated, vehicle-treated, and JQ1-treated *Myh6-Cre*:*Lmna*$^{F/F}$ mouse hearts. Nuclei were counterstained with DAPI. **B.** Corresponding quantitative data showing percentage of TUNEL-labeled nuclei in the myocardial sections in untreated (black dots; N=6), vehicle-treated (yellow dots; N=3) and JQ1-treated (orange dots; N=3) WT, and untreated (red dots; N=5), vehicle-treated (blue dots; N=7) and JQ1-treated (green dots; N=6) *Myh6-Cre*:*Lmna*$^{F/F}$ mouse hearts. P values were calculated using 2-way ANOVA and Tukey *post hoc* test for comparisons where *: $p < 0.05$, **: $p < 0.01$, ***: $p < 0.001$, ****: $p < 0.0001$. **C.** Transcript levels of selected BRD4 target genes involved in apoptosis, as quantified by RT-qPCR, are depicted in 3-weeks old untreated (black dots; N=4) and JQ1-treated (orange dots; N=5) WT mice, and in untreated (red dots; N=6), and JQ1-treated (green dots; N=8) *Myh6-Cre*:*Lmna*$^{F/F}$ mouse hearts. P values shown were obtained with Ordinary One-way ANOVA or Kruskal-Wallis where *: $p < 0.05$, **: $p < 0.01$, ***: $p < 0.001$, ****: $p < 0.0001$.

TABLE 1

Echocardiographic parameters in WT and *Myh6-Cre:Lmna*$^{F/F}$ untreated, vehicle and JQ-treated mice at 3 weeks of age.

	WT			***Myh6-Cre*:*Lmna*$^{F/F}$**			*p* value		
Groups	Untreated	Vehicle-Treated	JQ1-Treated	Untreated	Vehicle-Treated	JQ1-Treated	Interaction	Treatment	Genotype
N	12	10	11	16	11	22			
M/F	4/8	3/7	7/4	8/8	7/4	11/11			
Age (days)	21.5±1.0	21.1±1.0	21.4±0.7	20.9±1.3	20.6±0.5	21.0±0.5	0.85	0.38	0.02
BW (g)	9.5±2.6	10.0±1.5	8.4±2.6	9.0±0.7	9.5±1.2	8.6±1.2	0.95	0.009	0.26
HR (bpm)	464±52	446±33	436±32	479±77	477±37	492±51	0.40	0.70	0.006
ST (mm)	0.56±0.1	0.55±0.1	0.50±0.1	0.51±0.5	0.47±0.1	0.42±0.1*#	0.84	0.046	0.003
PWT (mm)	0.60±0.1	0.64±0.1	0.66±0.1	0.48±0.1#†	0.49±0.1#†	0.47±0.1*#†	0.59	0.44	<0.0001
LVEDD	2.92±0.4	3.05±0.3	2.57±0.6	3.50±0.5*†	3.78±0.3*#†	3.32±0.5†§	0.86	0.001	<0.0001
LVEDDi (mm/g)	0.32±0.0	0.31±0.1	0.32±0.1	0.39±0.0*#†	0.40±0.0*#†	0.39±0.1*#†	0.85	0.71	<0.0001
LVESD (mm)	1.69±0.3	1.83±0.3	1.45±0.5	3.08±0.6*#†	3.39±0.4*#†	2.51±0.7*†‡§	0.17	<0.0001	<0.0001
LVESDi (mm/g)	0.18±0.0	0.19±0.0	0.18±0.0	0.34±0.1*#†	0.36±0.0*#†	0.29±0.1*#†§	0.16	0.051	<0.0001
LVFS (%)	42.1±6.7	40.3±4.7	44.5±8.3	12.8±9.0*#†	10.7±3.4*#†	25.5±9.6*#†‡§	0.004	<0.0001	<0.0001
LVM (mg)	37.5±13.7	41.0±8.2	30.4±11.3	41.7±13.6	45.6±9.5†	33.1±7.3§	0.88	0.0006	0.16
LVMi (mg/g)	3.9±1.2	4.1±0.7	3.6±0.6	4.6±1.3	4.8±0.8	3.9±0.8	0.82	0.07	0.009

χ^2 was used to compare the M/F distribution; Data were analyzed by Two-way ANOVA followed by Bonferroni test for pairwise comparison, where: *: $p < 0.05$ for comparing untreated WT *vs* untreated, Vehicle-treated or JQ1-treated *Myh6*-Cre:*Lmna*$^{F/F}$

#: $p < 0.05$ for comparing Vehicle-treated WT *vs* untreated, Vehicle-treated or JQ1-treated *Myh6*-Cre:*Lmna*$^{F/F}$

†: $p < 0.05$ for comparing JQ1-treated WT *vs* untreated, Vehicle-treated or JQ1-treated *Myh6*-Cre:*Lmna*$^{F/F}$

‡: $p < 0.05$ for comparing Untreated *Myh6*-Cre:*Lmna*$^{F/F}$ *vs* JQ1-treated *Myh6*-Cre:*Lmna*$^{F/F}$

§: $p < 0.05$ for comparing Vehicle-treated *Myh6*-Cre:*Lmna*$^{F/F}$ *vs* JQ1-treated *Myh6*-Cre:*Lmna*$^{F/F}$

Abbreviations: HR, heart rate; bpm, beats per minute; ST, interventricular septal thickness; PWT, posterior wall thickness; LVEDD, left ventricular end diastolic diameter; LVEDDi, LVEDD indexed to body weight; LVESD, left ventricular end systolic diameter; LVESDi, LVESD indexed to body weight; LVFS, fractional shortening; LVM, left ventricular mass; LVMi, LVM indexed to body weight.